

# On the Nature and Genesis of EUV Waves: A Synthesis of Observations from SOHO, STEREO, SDO, and *Hinode*

Spiros Patsourakos<sup>1</sup> · Angelos Vourlidas<sup>2</sup> ·

© Springer ●●●

**Abstract** A major, albeit serendipitous, discovery of the *Solar and Heliospheric Observatory* mission was the observation by the *Extreme Ultraviolet Telescope* (EIT) of large-scale Extreme Ultraviolet (EUV) intensity fronts propagating over a significant fraction of the Sun's surface. These so-called EIT or EUV waves are associated with eruptive phenomena and have been studied intensely. However, their wave nature has been challenged by non-wave (or pseudo-wave) interpretations and the subject remains under debate. A string of recent solar missions has provided a wealth of detailed EUV observations of these waves bringing us closer to resolving their nature. With this review, we gather the current state-of-art knowledge in the field and synthesize it into a picture of an EUV wave driven by the lateral expansion of the CME. This picture can account for both wave and pseudo-wave interpretations of the observations, thus resolving the controversy over the nature of EUV waves to a large degree but not completely. We close with a discussion of several remaining open questions in the field of EUV waves research.

**Keywords:** Corona, Active; Coronal Mass Ejections, Low Coronal Signatures; Waves, Magnetohydrodynamic; Waves, Propagation; waves, Plasma

## 1. Introduction

One of the most important, as well as intriguing, discoveries of EIT (Delaboudinière *et al.*, 1995) on-board the *Solar and Heliospheric Observatory* (SOHO) were the EIT or EUV waves (Moses *et al.*, 1997; Thompson *et al.*, 1998, 1999). These are brightness fronts which propagate over significant fractions of the solar disk, mostly over quiet Sun (QS) areas, at speeds which can reach several hundred km s<sup>-1</sup> (e.g. Thompson and Myers, 2009). EUV waves are associated with

---

<sup>1</sup> University of Ioannina, Dept Physics-Section  
Astrogeophysics, GR 451 10 Ioannina, Greece email:  
spatsour@cc.uoi.gr

<sup>2</sup> Space Science Division, Naval Research Laboratory,  
Washington, DC 20375, USA

---

large-scale eruptive phenomena like flares and coronal mass ejections (CMEs). The sources of EUV waves lie within active regions (ARs).

A large statistical survey of EUV wave observations from EIT by Biesecker *et al.* (2002) showed a high degree of correlation between EUV waves and CME onsets for well-defined EUV waves; this was not the case for flares. Furthermore, Chen (2006) studied a set of energetic flares ( $\geq$  M GOES class) and found that only the eruptive ones were associated with EUV waves. On the other hand, weak flares (A and B GOES class), are often associated with EUV waves, whenever they are eruptive. From all the above we conclude that the existence of a CME is a strong condition for the occurrence of an EUV wave.

Several mechanisms have been suggested to explain the nature of EUV waves: (1) “*true*” waves (e.g. fast-mode waves), (2) *pseudo-waves* (e.g., compression fronts, current shells, and reconnection fronts around and/or at erupting flux ropes and (3) *hybrid*, i.e. a combination of both wave and pseudo-wave components. Examples from these mechanisms are given in Figure 1.

The *wave* interpretation asserts that EUV waves are “true” wave phenomena; namely, a fast-mode wave that is (most likely) triggered by a CME (e.g., Thompson *et al.*, 1998, 1999; Wang, 2000; Wu *et al.*, 2001; Ofman and Thompson, 2002). Such waves have two attractive properties: (i) they can propagate perpendicularly to the magnetic field and thus travel across the solar surface and (ii) they are compressive waves and hence can be detected in EUV images. Their typical speeds (200-400 km s<sup>-1</sup>) are in the range of the anticipated fast-mode speeds over QS. Another suggestion in the frame of the wave scenario, is that EUV waves are solitary waves, i.e. solitons (Wills-Davey, DeForest, and Stenflo, 2007).

The *pseudo-wave* interpretation suggests that EUV waves are not true wave phenomena, but rather the disk projection of the CME’s expanding envelope (Delannée and Aulanier, 1999). In this envelope, the plasma is been compressed by the flanks of the expanding CME flux rope and/or heated and compressed in a current shell around or at the surface of the erupting CME flux rope (to ensure current neutrality in the former case) (e.g., Delannée, 2000; Delannée *et al.*, 2008). Another variant of a pseudo-wave is that the CME flux rope laterally expands across the solar surface with a series of magnetic reconnections between the rope magnetic fields and QS magnetic fields of favorable orientation. These, presumably low-energy, reconnections cause transient brightenings which can give the appearance of an EUV wave, when collectively perceived (Attrill *et al.*, 2007a,b).

A third interpretation, the *hybrid* wave, tries to bridge the previous two opposing views, by first acknowledging that multiple bright fronts can be sometimes seen during events with EUV waves. Although this fact is quite obvious to anyone familiar with the observations, it is not always discussed clearly in the literature. According to the *hybrid* interpretation, there are two ‘EUV waves’. A sharp outer front consistent with a fast-MHD shock and considered the coronal counterpart of the Moreton wave, and an inner diffuse front consistent with a pseudo-wave and considered the ‘typical’ EUV wave (Chen *et al.*, 2002; Chen, Fang, and Shibata, 2005; Zhukov and Auchère, 2004; Cohen *et al.*, 2009; Pomoell, Vainio, and Kissmann, 2008). The latter is the key weakness of this interpretation, as

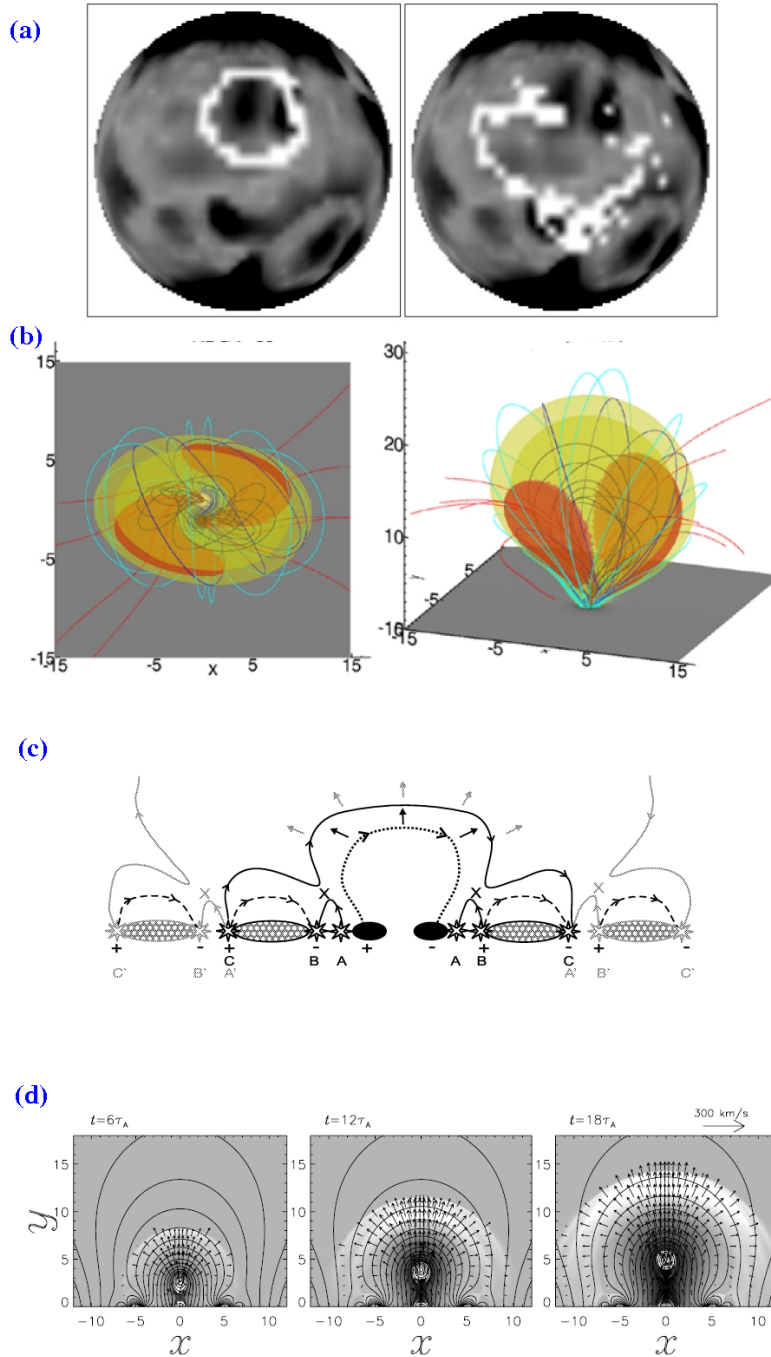


**Figure 1.** Proposed Physical Mechanisms for EUV waves. MHD fast-mode wave, (panel (a), from Wang (2000)). Pseudo-wave - current shell (panel (b), from Delannée *et al.* (2008)), pseudo-wave - reconnection front, (panel (c), from Attrill *et al.* (2007a)); hybrid pseudo-wave + MHD wave/shock, (panel (d), from Chen *et al.* (2002)). Panels (a), (c) and (d) reproduced by permission of the AAS.

---

we will discuss later. While accepting the existence of two fronts on theoretical grounds, the hybrid interpretations tend to dismiss the observational detection of two fronts for a given event in favor of a single front associated with the expanding CME (or the surrounding field). As we will discuss in Section 12, this is not the complete picture. The two fronts exist, they are observed, and recent theoretical work sheds a much clearer light in this *hybrid* view (Downs *et al.*, 2011).

At this point we should emphasize that observations reveal a large diversity of moving features in association with the EUV wave. This becomes evident when the image cadence, observational lines of sight, and temperature coverage are increased throughout the solar atmosphere. The long list of observed features includes expanding loops, mass flows, core and extended dimmings, stationary brightenings, deflections, and oscillations of ambient coronal structures. These manifestations occur in tandem to the large-scale front which is essentially the EUV wave. Moreover, EUV waves are frequently associated with phenomena observed in other wavelength domains such as Moreton waves in the chromospheric H $\alpha$  (e.g., Thompson *et al.*, 2000; Warmuth *et al.*, 2001) and He I 10830 Å lines (e.g., Vršnak *et al.*, 2002), and in the corona in Soft X-rays (SXR) (e.g., Khan and Aurass, 2002; Hudson *et al.*, 2003; Warmuth, Mann, and Aurass, 2005) microwaves (e.g., Warmuth *et al.*, 2004; White and Thompson, 2005) and in the metric-range (e.g., Vršnak *et al.*, 2005).

We also note that there is a hierarchy of EUV waves. The higher cadence and sensitivity of the EUVI and AIA observations showed the existence of small-scale waves which are associated with and are probably triggered by small-scale eruptions, like small erupting filaments, (e.g., Innes *et al.*, 2009; Podladchikova *et al.*, 2010; Zheng *et al.*, 2011; Zhang and Liu, 2011). The speeds of these "mini-waves" range between 10 and 250 km s<sup>-1</sup> and the waves leave small dimmings behind them. However, they do not reach the global scales that "ordinary" EUV waves since they travel over distances of the order of around 100 Mm only. In this paper, we will deal exclusively with *global* EUV waves, i.e. well-developed, clearly visible (at least initially) propagating fronts which reach distances of a significant fraction of the solar radius. This is in our opinion an objective criterion because it does not depend on the derived speed of the propagating disturbance which seems to be sometimes a function of image cadence. For example, EIT captured only the slower of EUV waves, due to its low-cadence, as was revealed by the higher cadence STEREO/SECCHI (Howard *et al.*, 2008) observations (Long *et al.*, 2008; Veronig, Temmer, and Vršnak, 2008).

EUV waves comprise a very active field of coronal research which is characterized by occasional controversy and intense debate. Consequently, the subject has been reviewed extensively over the years. Recent reviews on EUV waves can be found in Warmuth (2007); Wills-Davey and Attrill (2009); Warmuth (2010); Gallagher and Long (2011) and Zhukov (2011). We first focus on multi-viewpoint observational results (this is a 'Sun-360' Topical Issue, after all), discuss energetics, and finally propose a top-level synthesis of the CME-EUV wave interplay that, we believe, accounts for the majority of the observations and can resolve past controversies. Of course, we update the field with as many recent publications as we could. We start with a review of the kinematics and coronal

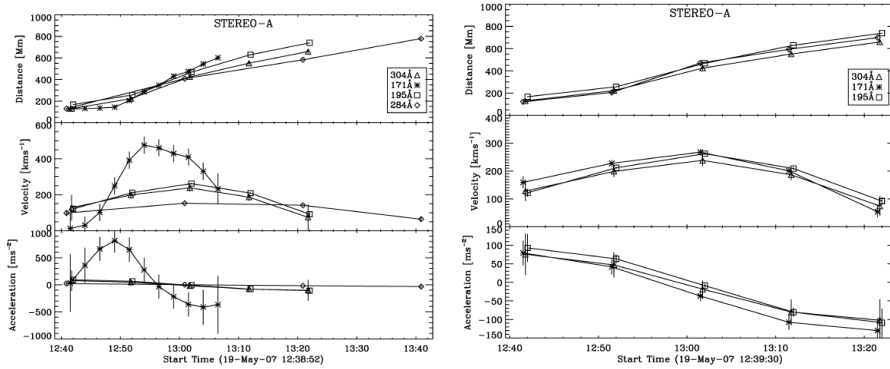


**Figure 2.** Time evolution of distance, speed and acceleration for an EUV wave which took place on 19 May 2007. Left panel has 171 channel observations at 2.5 minute cadence while right panel at a reduced 10 minute cadence. From Long *et al.* (2008). Reproduced by permission of the AAS.

interactions of the waves, proceed to the thermal and 3D structure, and then discuss associated phenomena, such as brightenings, ripples, etc, that can lead to confusion. We then turn our attention to two rarely-discussed subjects; namely, the spectroscopic observations and energetics of EUV waves. In Section 10-11, we synthesize the current knowledge on this phenomenon by first discussing the genesis of EUV waves and then describe a picture of the CME-EUV wave connection that seems to be consistent with the majority of the observations. We conclude in Section 12 with a list of open questions and possible areas of research in near-future. We concentrate on recent observations acquired by space missions, such as SOHO, Hinode, STEREO and SDO. We use the term EUV wave throughout the paper regardless of the physical interpretation ("true" wave or pseudo-wave) of the phenomenon.

## 2. Kinematics, Amplitudes and Dispersion

Arguably the best studied property of EUV waves is their kinematics. The steady increase in image cadence, from 720 s with SOHO/EIT to 150 s with EUVI on STEREO/SECCHI, and finally to 12 s with SDO/AIA, is the key factor for improving our understanding. 'Point-and-click', semi-, and fully-automated methods are used to determine the time-distance curve ( $t-d$ ) or ground-track of the wave in one or more angular sectors. Then, simple numerical derivation or fittings of the ( $t-d$ ) curves with various functions provide the speed and acceleration profile of the wave.

The first STEREO/EUVI detailed kinematic observations of an EUV wave on 19 May 2007 by Long *et al.* (2008) and Veronig, Temmer, and Vršnak (2008) showed that the lower cadence of EIT *underestimated* the initial speeds of the waves. The higher EUVI cadence revealed significant *deceleration* of the first wave fronts from  $\approx 400 \text{ km s}^{-1}$  to  $200 \text{ km s}^{-1}$  in a matter of almost 10 minutes; after this interval the wave was traveling at an almost constant speed of about 200

---

km s<sup>-1</sup> (left panel of Figure 2). Lower cadence observations would have missed significant part of the deceleration phase (right panel of Figure 2). For higher initial wave speeds (>400-500 km s<sup>-1</sup>) even the EUVI cadence is inadequate. The first EUV wave observations by AIA (Lemen *et al.*, 2012) showed examples of EUV waves with very high initial speeds (650-2000 km s<sup>-1</sup>) undergoing large decelerations, up to  $-2.0 \times 10^3 \text{ m s}^{-2}$  (Chen and Wu, 2011; Ma *et al.*, 2011; Kozarev *et al.*, 2011; Liu *et al.*, 2011; Cheng *et al.*, 2012; Olmedo *et al.*, 2012).

Compilation of the kinematics of other events observed by EUVI and AIA showed either waves experiencing significant deceleration in their early stages (e.g., Kozarev *et al.*, 2011; Long *et al.*, 2011; Ma *et al.*, 2011; Muhr *et al.*, 2011; Warmuth and Mann, 2011) or waves with  $\approx$  constant speeds (e.g., Kienreich, Temmer, and Veronig, 2009; Ma *et al.*, 2009; Patsourakos *et al.*, 2009; Patsourakos and Vourlidas, 2009; Temmer *et al.*, 2011; Kienreich *et al.*, 2011; Liu *et al.*, 2010; Long *et al.*, 2011; Warmuth and Mann, 2011). Irrespective of their initial speeds or deceleration profiles, these waves ended up travelling within a rather narrow speed range of 180-380 km s<sup>-1</sup> which is consistent with the fast mode speed over the quiet Sun (e.g., Wang, 2000; Wu *et al.*, 2001; Warmuth and Mann, 2005; Cohen *et al.*, 2009; Schmidt and Ofman, 2010; Downs *et al.*, 2011; Zhao *et al.*, 2011). Therefore, the kinematics of the observed waves are consistent with fast-mode waves. Such waves are initially driven and even shocked sometimes (for the fast and decelerating events) with their initial speeds reflecting the speed of the driver and not the characteristic speed of the medium where they propagate. Note here that all these events correspond to "truly" global waves since they cover distances 350-850 Mm, or conversely 0.5-1.3 R<sub>⊙</sub>; these waves were also "well-observed" events showing clear evidence of propagation of well-defined fronts.

At this point it will be useful to discuss some of the key properties of both linear and non-linear fast mode waves, and their kinematic behavior in particular. Detailed discussions on this topic can be found in Mann (1995); Vršnak and Lulić (2000); Warmuth (2007). Waves with large amplitudes, shocks being a special case, cannot be treated linearly and their speeds are always higher than the ambient fast-mode speed profile. Their kinematics would depend on the wave amplitude. When energy input ceases (i.e. blast-wave), the wave decelerates when traveling in a constant fast-mode speed medium since its amplitude is decreasing due to profile broadening and geometrical expansion. On the other hand, when a non-linear wave is still driven, due to the expanding CME acting as a piston, for example, its amplitude increases, and therefore it accelerates. When the amplitude of the disturbance is small, we have linear waves travelling at the characteristic speed of the medium. Therefore, linear waves would follow the fast-mode speed profile of the ambient medium and would travel at constant speeds for uniform fast-mode profile, as expected for propagation over QS areas. However, linear waves could also experience acceleration or deceleration when they cross the boundaries between regions with strong fast-mode speed gradients, like QS, coronal holes or ARs (see Section 3). In conclusion, both linear and non-linear fast-mode waves could exhibit constant speed, accelerating and decelerating kinematic profiles and should reflect or dissipate at coronal hole or AR boundaries.

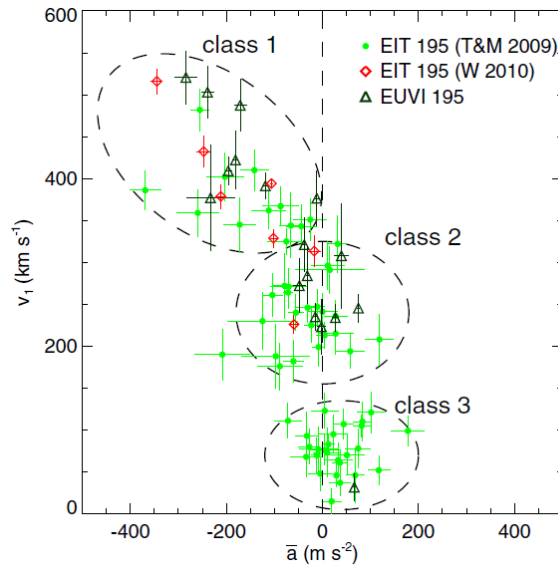


**Figure 3.** Statistical relationship between initial EUV wave speed and average acceleration for 17 waves observed by EUVI and 61 waves observed by EIT. From Warmuth and Mann (2011). Credit: Warmuth, A., Mann, G., *A&A*, 532, 151, 2011, reproduced with permission ©ESO.

This behavior has been put into a broad context with the recent extensive statistical study of Warmuth and Mann (2011) where the kinematics of a comprehensive set of EUV waves (61 observed by EIT and 17 observed by EUVI) has been used. Most of the EIT observations were from a catalog of 176 EUV waves compiled by Thompson and Myers (2009). Figure 3 shows the initial wave speed against the mean wave acceleration. For initial wave speeds exceeding roughly  $320 \text{ km s}^{-1}$  there is a clear trend that faster waves experience stronger decelerations (class 1 in Figure 3). Waves with intermediate speeds ( $\approx 170\text{--}320 \text{ km s}^{-1}$ ) are characterized by small magnitude accelerations or decelerations which is consistent with  $\approx$  constant speed (class 2 in Figure 3). Finally, very slow waves (speeds  $< 120 \text{ km s}^{-1}$ ) exhibit small accelerations/decelerations (class 3 in Figure 3). It is unlikely that the fast-mode wave interpretation applies in these cases since their speeds are smaller or of the same order as the coronal sound speed, and the fast-mode speed depends on the quadratic sum of the sound and the Alfvén speeds. These slow waves are consistent with pseudo-wave interpretations although a slow-mode wave travelling at almost  $90^\circ$  with respect to the ambient magnetic field is another possibility Podladchikova *et al.* (2010). Another clue to the non-wave nature of the slow EUV waves is that they do not cover big distances during their lifetimes, so they cannot qualify as global waves. One example of a slow pseudo-wave was reported by Zhukov, Rodriguez, and de Patoul (2009). The measured time-speed profile (see Figure 4) was not smooth but exhibited a series accelerations and decelerations. In reality, the observed "EUV wave" was just the footprint of an erupting filament undergoing rotation.

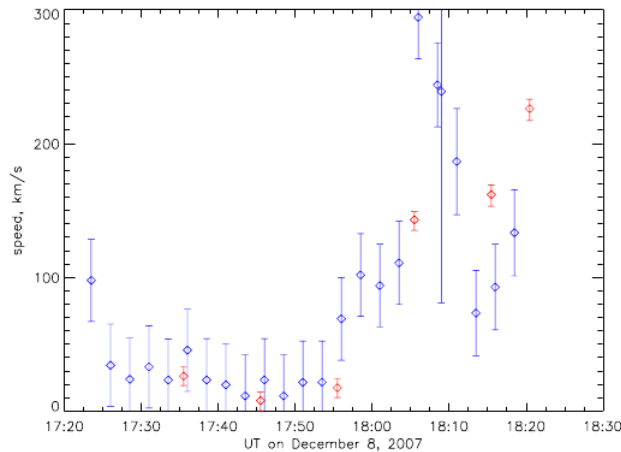


**Figure 4.** Time-speed plot for an EUV wave which took place on 8 December 2008 exhibiting erratic kinematic behavior. From Zhukov, Rodriguez, and de Patoul (2009).

This example highlights the importance of analyzing the wave kinematics in order to deduce the nature of the observed waves.

The study of the *perturbation profiles* ( $pp$ ) of EUV waves is another powerful tool. Although different definitions can be found in the literature, a  $pp$  profile essentially measures the intensity distribution across the wave,  $I(r, t)$ , with respect to the distribution,  $I(r, t_0)$ , at a pre-wave moment  $t_0$ . It is  $pp \propto I(r, t)/I(r, t_0)$ , where  $r$  is the distance from a fixed initiation point of the wave. For any given time, the maximum and the  $FWHM$  of the  $pp$  are deduced by fitting the  $pp$  with a Gaussian profile, for example.

The  $pp$  analysis of EUV waves resulted in several interesting findings (Veronig *et al.*, 2010; Long *et al.*, 2011; Muhr *et al.*, 2011). The wave  $FWHM$  is generally an *increasing* function of distance. At the same time, the wave amplitude  $A$  (i.e. peak value of the  $pp$ ) *decreases* with time. The  $pp$  analysis of EUV waves and of the associated Moreton waves by Warmuth (2010) showed they both exhibit profile broadening and amplitude decrease. For some events, the integral of  $pp$  over distance which is proportional to  $A \times FWHM$  is constant or decreases with distance. All the above suggest that the observed disturbances are consistent with freely-propagating (blast) waves since the total energy is either constant (constant  $A \times FWHM$ ) or decreasing (decreasing  $A \times FWHM$ ). The pulse broadening points also to a freely-propagating wave. Indeed, Grechnev *et al.* (2011) found that a 3D model of a blast wave propagating in a medium with density stratification was broadly consistent with the ground track of 17 January 2010 (see also Veronig *et al.* (2010)). Finally, MHD modeling of rotating sunspots by Selwa, Poedts, and DeVore (2012) showed that dome-like structures, similar to what is observed, could be generated.

A recent study of a wave which took place on 14 August 2010 and was observed by AIA allowed to deduce the wave dispersion characteristics with ultra-high cadence and at multiple channels (Long, DeLuca, and Gallagher, 2011). The AIA observations showed that the wave width increases with time in all channels



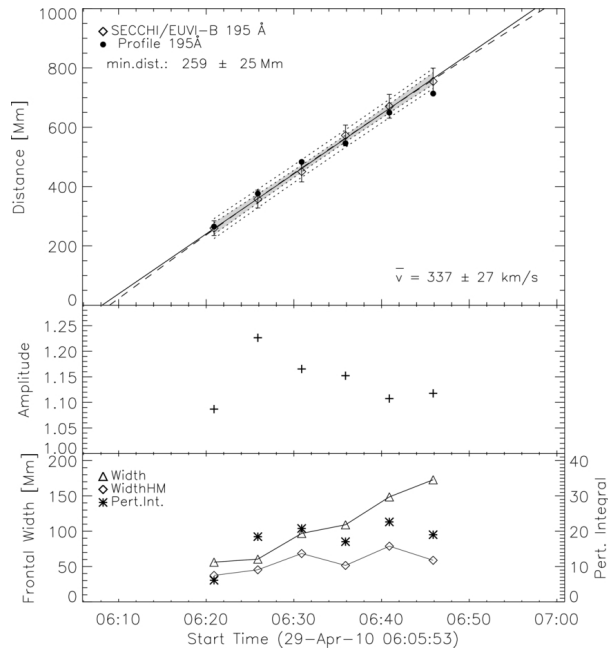


**Figure 5.** Analysis of perturbation profiles of an EUV wave which took place on 10 April 2010. Time evolution of wave distance (upper panel), wave amplitude (middle panel) and wave width and perturbation integral (lower panel). From Muhr *et al.* (2011). Reproduced by permission of the AAS.

while its magnitude was decreasing. By treating the  $pp$  of the waves as a linear combination of sinusoidal waves within a Gaussian envelope, Long, DeLuca, and Gallagher (2011) found a dispersion rate of the pulse of  $8\text{-}13 \text{ Mm}^2\text{s}^{-1}$ . The dispersive nature of the observed wave is a strong indication for its wave nature. Wave dispersion is at odds with solitary waves.

Kienreich *et al.* (2011) presented the first observations of *homologous* EUV waves; within a period of 10 hours during April 28-29 2010 four EUV waves were launched from the same AR and along the same direction. This basically ensures that these waves propagated over more or less the same background coronal conditions (i.e., plasma  $\beta \approx \text{constant}$ ). It was found that the faster the wave the larger the corresponding maximum compression ratio  $X_c (\propto (I/I_0)^{1/2})$ . Kienreich *et al.* (2011) calculated the corresponding magnetosonic Mach numbers  $M_{ms} = f(X_c, \beta)$  from the observed compression ratios for each event and found they were strongly correlated with the (linear) wave speed. This result provided strong support that the observed waves were indeed fast-mode shocked (non-linear) waves.

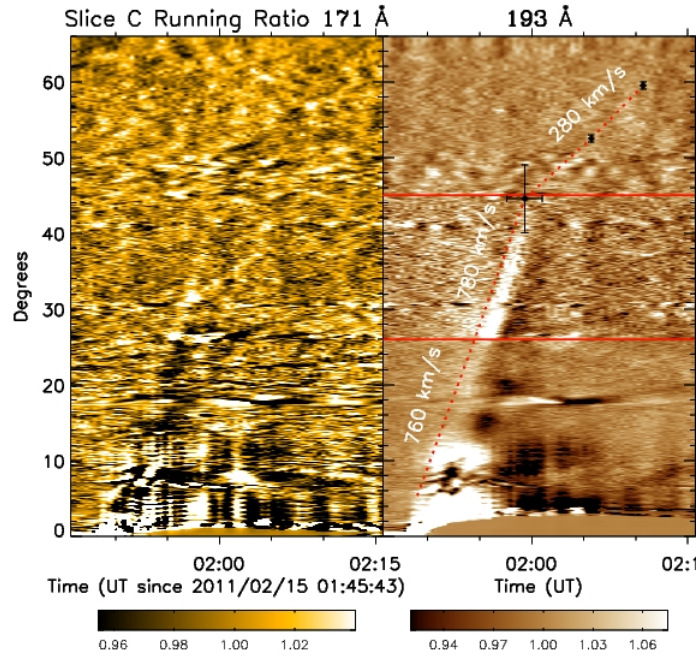


**Figure 6.** Combined AIA-EUVI observations of wave reflection and transmission. Time-angle plot along a given direction of an EUV wave which took place on 15 February 2011. Red dots are the wave ground tracks and the two horizontal red lines define a coronal hole. From Olmedo *et al.* (2012). Reproduced by permission of the AAS.

### 3. Interactions with the ambient corona: reflections, transmissions and oscillations

MHD waves, as any type of wave, must follow the basic rules of optics. This means that at least part of the wave could be reflected away from places of strong gradients in the characteristic speed of the medium where they propagate. For the case of the fast-mode speed, strong gradients are expected at the interfaces between QS and coronal holes and ARs where the fast-mode increases from few hundred  $\text{km s}^{-1}$  to several hundred or even thousand  $\text{km s}^{-1}$  (e.g., Wang, 2000; Schmidt and Ofman, 2010). Wave transmission through a coronal hole could occur when a resonance between the coronal hole and the incoming wave takes place (Schmidt and Ofman, 2010). The EUV wave simulations of Wang (2000) and Schmidt and Ofman (2010) showed wave reflection from the boundaries of coronal holes.

The EUVI observations of the 19 May 2007 wave by Gopalswamy *et al.* (2009) showed evidence of wave reflection from a small equatorial coronal hole. The speed of the reflected wave was similar to the speed of the incoming wave. The reported reflection was put into some question by Attrill (2010), based on the running-difference images used in the Gopalswamy *et al.* (2009) analysis. It is true that running-differences could lead to some confusion, particularly when one is looking at reflections since these occur over regions which are already

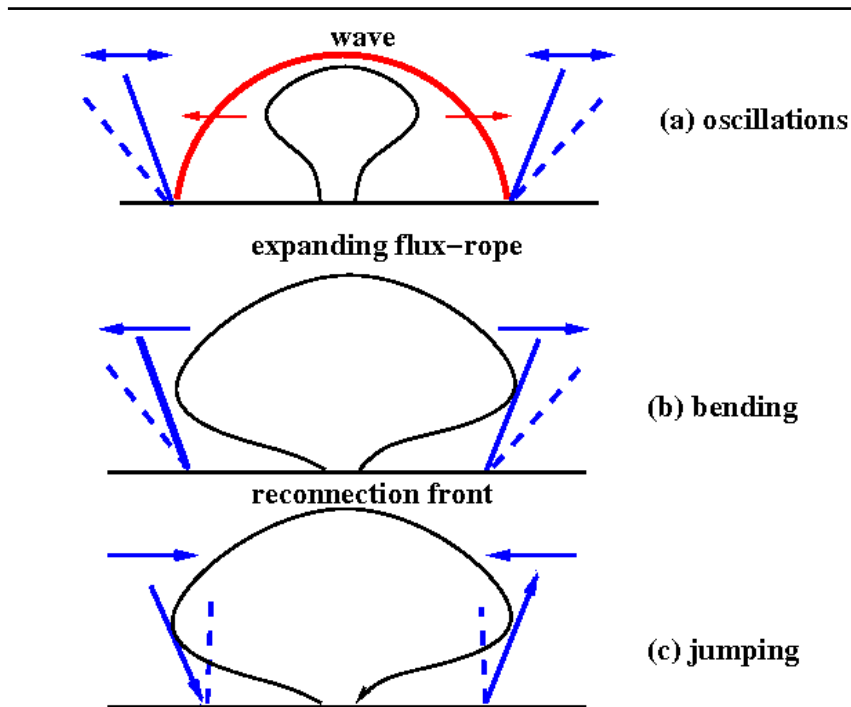


**Figure 7.** Expected interactions between EUV waves and ambient coronal structures in the frame of the various physical mechanisms proposed for EUV waves. The mushroom-shaped object is the laterally and radially expanding CME structure. The inclined solid blue lines represent ambient coronal structures before the interaction with the wave or CME. The inclined dashed blue lines represent the new locations of the ambient coronal structures after the interaction. The blue arrows show the direction of motion of the ambient structures induced by the interaction. Upper panel: Wave mechanism. The expanding CME launches a wave (red) which sets the ambient coronal structures into oscillations. Middle panel: CME Current-shell, CME-compression front mechanism. There is no wave. The expanding CME pushes the ambient coronal structures *continuously* as it expands. No oscillations should be produced. Lower panel: Reconnection mechanism. No wave is produced. The expanding CME reconnects with the ambient structures of opposite polarity which should then “jump” inwards. No oscillations should be observed.

perturbed by the incoming wave. However evidence of wave reflection for this event is also seen in the direct images.

The angular separations between the two STEREO and the SDO spacecraft provided for the first time a 360-degree coverage of an EUV wave which took place on 15 February 2011 (Olmedo *et al.*, 2012). The source AR was close to the central meridian and wave tracks travelling both towards the southeast and the southwest were reflected off an extended south pole coronal hole. In addition, part of the wave was *transmitted* through the coronal hole rather than reflected (see Figure 6). The wave approached the hole with a speed of  $760 \text{ km s}^{-1}$ ; the transmitted part traveled within the coronal hole at a speed of  $780 \text{ km s}^{-1}$ , once the wave either reflected off or exited through the coronal hole it traveled at a slower speed of around  $280 \text{ km s}^{-1}$ . This kinematic behavior fits nicely with a wave interpretation. An initially driven wave (incoming wave) reaches the coronal hole and part of it is reflected by the strong fast-mode

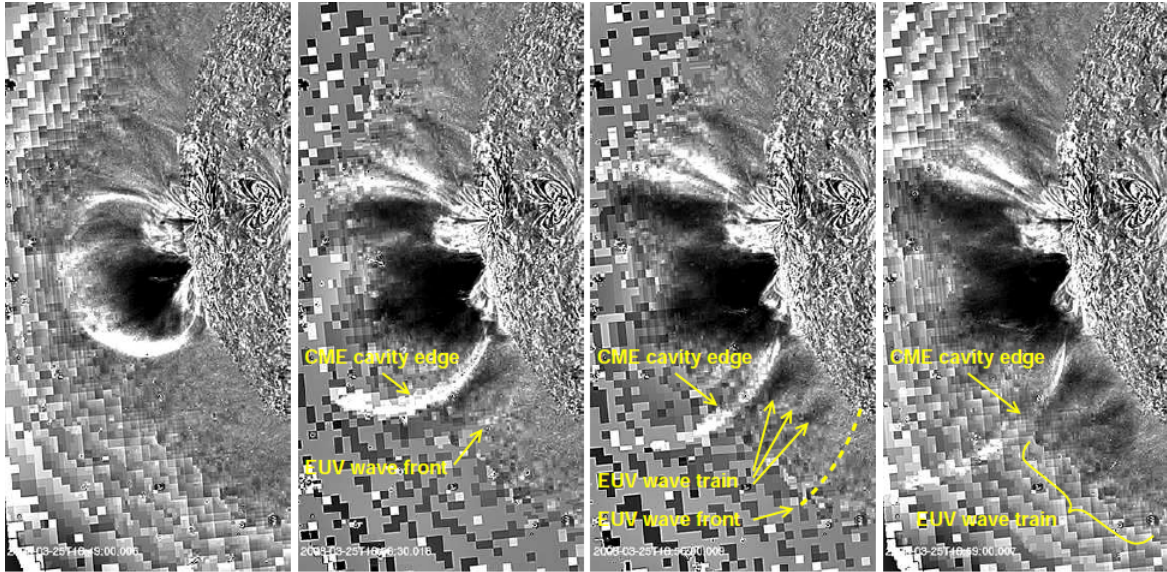


**Figure 8.** Deflections of ambient coronal structures from the impact of an EUV wave which took place on 25 March 2008. From Patsourakos, Vourlidas, and Kliem (2010). Credit: Patsourakos, S., Vourlidas, A., Kliem, B., 522, 100, 2010, reproduced with permission ©ESO.

speed gradient of the coronal hole and part is transmitted through it. The faster propagation speed within the coronal hole correlates with the higher fast-mode speeds within coronal holes; the slower speeds of the reflected and transmitted waves which travel over QS are consistent with typical QS fast-mode speeds. The observed very fast wave transmission through a coronal hole makes it possible that pre-SDO observations could have missed similar effects in other events (i.e. the wave transit time through the hole is only 5 minutes). Wave reflection and transmission through a coronal hole are hard to reconcile with pseudo-waves since CMEs never propagate into coronal holes for example. Transmission into coronal holes is sometimes observed for Moreton waves as well (Veronig *et al.*, 2006).

Motions in the form of deflections/oscillations of ambient coronal structures are another important indicator of the nature of EUV waves. Looking at any high cadence off-limb movie of EUV waves (e.g., Patsourakos and Vourlidas, 2009; Patsourakos, Vourlidas, and Kliem, 2010) one sees evidence of oscillations of ambient coronal structures which are set up once the wave impinges on them (e.g. Figure 8). The outermost oscillating structures roughly outline the locations of the wave front. To illustrate this effect we included as electronic supplement a 193 AIA channel base-ratio movie of the event of the 13 June 2010. In the southern part of the eruption we note an area growing with time which exhibits oscillations of off-limb structures. These are manifested as alternating black-and-white stripes at any given location. The most natural explanation for these oscillations is that a true MHD wave impinges on the ambient coronal structures and sets up an oscillation (e.g. panel (a) of Figure 7). Similar deflection phenomena have been observed further away as streamer deflections with coronagraphs in connection

---

with CME-driven shocks (e.g., Gosling *et al.*, 1974; Sheeley, Hakala, and Wang, 2000; Vourlidas *et al.*, 2003). Vršnak *et al.* (2006) and Tripathi and Raouafi (2007) reported streamer deflections in direct temporal and spatial association with EUV waves.

On the other hand, if an expanding flux rope were responsible for these deflections, it should bend the ambient coronal structures rather continuously along the direction of its lateral expansion as it rolls over them (panel (b) of Figure 7). We would not observe oscillations in that case. Finally, a reconnection front (panel (c) of Figure 7) would cause opposite directed “jumps” (which could be interpreted as oscillations). Once again, the observations of oscillations of ambient structure support a wave-interpretation for EUV waves.

Other phenomena triggered by EUV waves are kink-like oscillations of disk filaments (Hershaw *et al.*, 2011) and coronal loops (e.g., Wills-Davey and Thompson, 1999; Aschwanden and Schrijver, 2011). The velocity of these transverse oscillations is in the range of 5-50 km s<sup>-1</sup>, the same range as filament oscillations triggered by Moreton waves (e.g., Gilbert *et al.*, 2008); for a review on filament/prominence oscillations and their dissipation mechanisms the interested reader can refer to Arregui and Ballester (2011). More recently, AIA observations of the 2011 June 7 event by Li *et al.* (2012) showed evidence of *secondary* waves triggered in nearby ARs or individual loop-like structures when the main wave hits them. Using the observed velocities, and typical masses and densities for filaments and coronal loops, one can estimate the kinetic energy associated with the oscillations (e.g., Ballai, Erdélyi, and Pintér, 2005). The deduced energies are rather small, in the range of nanoflares, and set a lower limit on the total energy of EUV waves.

#### 4. Thermal Structure

The first truly multi-thermal observations of EUV waves were achieved by EUVI, when the same EUV wave was observed in 4 different channels (171, 195, 284, 304) with cadence from 2.5-20 minutes (e.g., Long *et al.*, 2008; Veronig, Temmer, and Vršnak, 2008; Patsourakos *et al.*, 2009). The main result was that EUV waves are best observed in the 195 channel, which has a peak response temperature of about 1.5 MK. They are weaker in other channels.

AIA improved the study of the thermal structure of EUV waves by supplying observations at 12 s cadence in seven channels (94, 131, 171, 193, 211, 335, 304) sampling the transition region (0.08 MK), warm (1-3 MK) and flaring corona (6-10 MK). The AIA observations of Liu *et al.* (2010), Kozarev *et al.* (2011), Long, DeLuca, and Gallagher (2011), Ma *et al.* (2011) and Schrijver *et al.* (2011) showed that EUV waves are best seen in the 193, 211, 335 channels which implies temperatures in the range 1.0-2.5 MK (see for example Figure 9). On the other hand, EUV waves in the 171 channel (the cooler coronal channel) are sometimes manifested as intensity *depletions*, i.e. darkening, in contrast to the other coronal channels where wave fronts are bright. The 171 observations of intensity depletions associated with EUV waves imply that observations of a faint bright front in a 304 channel imply that the 304 signal comes from the

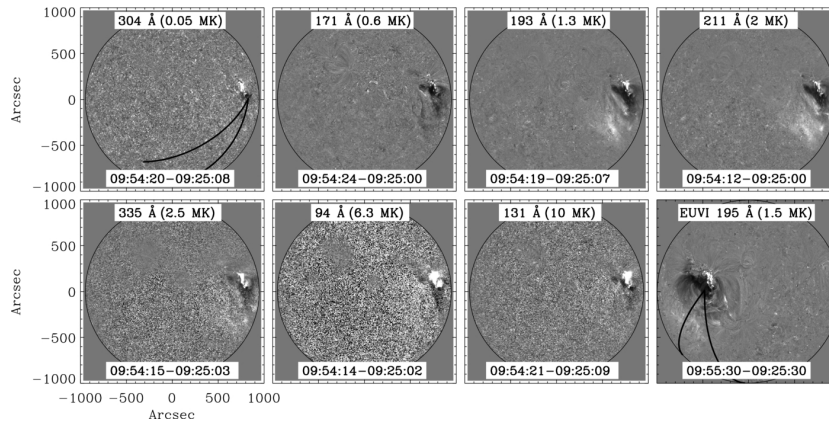


**Figure 9.** AIA observations of an EUV wave which took place on 14 August 2010 in several EUV channels. From Long, DeLuca, and Gallagher (2011). Reproduced by permission of the AAS.

corona (i.e., the Si XI line at  $303.32 \text{ \AA}$  in the 304 channel) and not from the transition region (i.e., He II  $304 \text{ \AA}$  line) as discussed in Patsourakos *et al.* (2009) and Long, DeLuca, and Gallagher (2011).

Schrijver *et al.* (2011) modeled the intensity changes associated with an EUV wave on 15 February 2011 using the temperature response functions of AIA and the assumption that the observed variations were due only to adiabatic compression. They found that the data were consistent with mild plasma heating and compression, a type of plasma “warming”. The estimated density and temperature increases were  $\approx 10 \%$  and  $\approx 7 \%$  respectively, while the “allowed” temperature range for the wave plasma was 1.2-1.8 MK.

Kozarev *et al.* (2011) and Ma *et al.* (2011) analyzed the thermal structure of an EUV wave on 13 June 2010. This event was associated with a type II metric radio shock. Kozarev *et al.* (2011) used the AIA intensities recorded in several coronal channels to perform Differential Emission Measure (DEM) analysis before and during the EUV wave. They found that during the wave the DEM is increasing for temperatures roughly exceeding the peak temperature of the pre-event DEM ( $\approx 1.8 \text{ MK}$ ). This implies both plasma heating and compression. Assuming no temperature change, they found a *lower* limit for the density increase in the range 12-18%. Ma *et al.* (2011) deduced from the dynamic radio spectrum of the associated shock a compression ratio (1.56) and from the AIA data the wave speed. Feeding these parameters to the jump conditions for a perpendicular MHD shock they found down-stream plasma heating to  $\approx 2.8 \text{ MK}$ . Using this temperature they found ionization time-scales roughly consistent with observed timescales of the EUV wave in the various AIA channels. This suggests that the observed EUV wave was consistent with a shocked wave.

## 5. 3D Structure and Relationship with CMEs

Multi-viewpoint observations using the two STEREO spacecraft or combinations of STEREO with SOHO or SDO can provide important geometrical characteris-

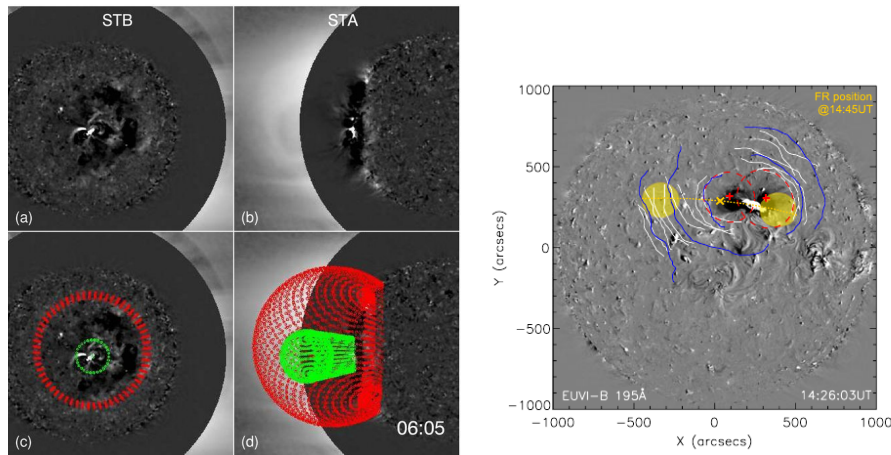


**Figure 10.** SECCHI multi-viewpoint observations and geometrical modeling of EUV waves and comparison with the associated CMEs. Left panel from Patsourakos and Vourlidas (2009) (13 February 2009 event) and right panel from Temmer *et al.* (2011) (26 April 2008 event). Left panel reproduced by permission of the AAS.

tics of EUV waves as well as the wave–CME association in the 3D space including their lateral extensions.

Triangulations using STEREO data of an EUV wave which occurred on 7 December 2007 derived a wave front height of  $\approx 90$  Mm (Patsourakos *et al.*, 2009). This is comparable to the coronal scale-height (70 Mm) at a temperature of 1.5 MK, which is the characteristic temperature of the EIT and EUVI 195 Å channels and of the AIA 193 Å channel. It may be the reason why EUV waves are usually best observed at this wavelength. The above height is indeed an “emission” height, i.e. the height from which the bulk of the wave emission originates. Wave emissions originating from higher altitudes will be weaker and possibly invisible (Robbrecht, Patsourakos, and Vourlidas, 2009) since the EUV emission has a strong dependence on density which falls off very rapidly with height. These arguments provide a strong constraint on the physical mechanism(s) of EUV waves because they must act at the base of the corona irrespective of their nature (wave or pseudo-wave) in order to give an observable signature.

3D geometrical modeling of the EUV wave envelope and of the associated CME as seen in the inner corona in the EUV or in white-light (WL) with coronagraphs (e.g., COR1 on SECCHI) casts light into the wave-CME relationship (Patsourakos *et al.*, 2009; Patsourakos and Vourlidas, 2009; Temmer *et al.*, 2011). For this task, widely separated views of the EUV wave and of the CME are used. Ideally one view is off-limb or close to the limb and the other is on-disk. The 3D forward geometrical model of Thernisien, Vourlidas, and Howard (2009) is used to obtain a 3D fit of the EUV wave and of the associated CME which are then projected onto the solar disk (e.g., Figure 10). The results reveal a *spatial offset* and *size disparity* between the projections of the EUV waves and their associated CMEs which indicates two possibly related (the wave running ahead of the CME) but *different* entities. Such results are clearly inconsistent with pseudo-wave models for which wave and CME are the same thing by definition.

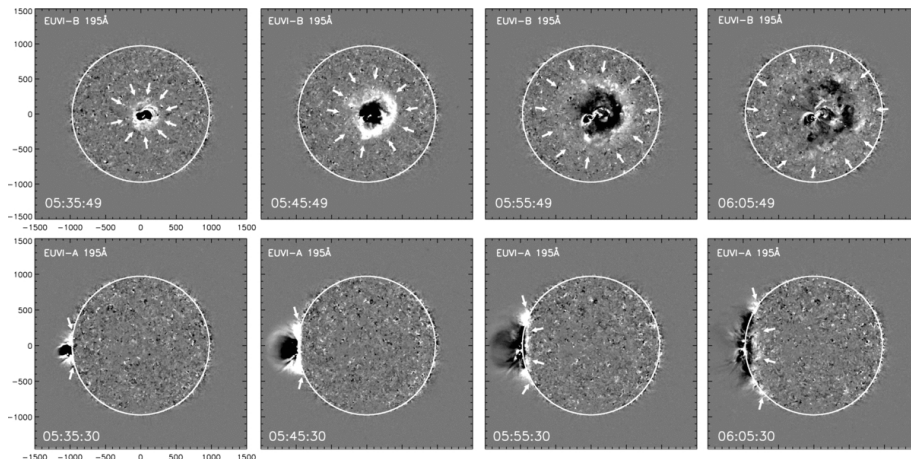


**Figure 11.** STEREO quadrature observations of an EUV which took place on 13 February 2009. Upper panel STEREO A observations with an EUV wave and associated CME view from above and lower panel STEREO B observations with an EUV wave and associated CME view from the side. Median-filtered running difference images are shown. From Kienreich, Temmer, and Veronig (2009). Reproduced by permission of the AAS.

The ultimate test for the relationship between EUV waves and CMEs became possible with the availability of *quadrature* STEREO observations of an event which took place on 13 February 2009 (Kienreich, Temmer, and Veronig, 2009; Patsourakos and Vourlidas, 2009), when the two STEREO spacecraft had a  $90^\circ$  separation. The source AR was located at disk center from STEREO B and at the east limb as seen from STEREO A (Figure 11). This is an ideal configuration for measuring the wave (disk view) and CME kinematics (limb-view) simultaneously (Figure 12). It was found that the wave and CME were initially co-spatial but they decoupled quickly with the wave detaching away from the CME flanks. The same conclusion was reached by Kienreich, Temmer, and Veronig (2009) from the analysis of off-limb maps of the event taken at several heights. They found that the start of lateral expansion of the EUV CME marked the initiation of the on-disk wave and that the expansion started at a height of  $\approx 90$  Mm. The observed behavior suggested an initially driven disturbance which eventually became a freely propagating MHD wave travelling at around  $250 \text{ km s}^{-1}$  (Kienreich, Temmer, and Veronig, 2009; Patsourakos and Vourlidas, 2009). These results, especially the decoupling of the wave from the CME front, have been recently verified with high cadence AIA observations in several events (Ma *et al.*, 2011; Cheng *et al.*, 2012).

Therefore, the CME front should follow the EUV wave front. But how can these results be reconciled with past reports of the exact opposite behavior (Vršnak *et al.*, 2006; Warmuth, 2010) or with the claims of a single front (Attrill *et al.*, 2009; Dai *et al.*, 2010)? In a nutshell and with the benefit of hindsight, these conflicting reports were cases of front misidentification due to poor wavelength and temporal coverage. There are only two reports of a CME front running ahead of an EUV wave (8 August 1998, 3 November 2003) and both of them were very poorly observed lacking LASCO or EIT observations. Hence, in the



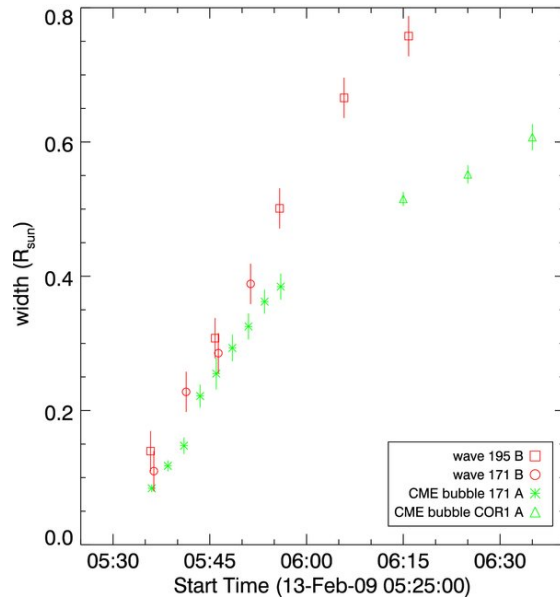


**Figure 12.** Distance time of the EUV wave (red symbols) from a disk-view and associated EUV-WL CME (green symbols) from an off-limb view for the quadrature observations of 13 February 2009. From Patsourakos and Vourlidas (2009). Reproduced by permission of the AAS.

case of the 3 November 2003 event, the CME front is assumed to be the soft X-ray front while the EUV wave is associated with the Moreton wave in  $H\alpha$ . But there is no independent proof that the CME and soft X-ray fronts are the same. Besides, there was a lot of SXR activity during this period which could easily mask the actual CME SXR front due to the flaring emission. For the cases where only one front is reported, the low cadence does seem to affect the interpretation. Dai *et al.* (2010) actually observe and comment on the existence of two fronts (their Figure 4) but they disregard the wave interpretation on the basis of the low lateral speed ( $260 \text{ km s}^{-1}$ ) compared to the speed of the CME ( $600 \text{ km s}^{-1}$ ). But these are exactly the speeds expected by an MHD wave far from the eruption and they lack the cadence to measure the much higher speeds at earlier times. Attrill *et al.* (2009) make the *a priori* assumption that the outer edge is the CME edge but they miss the outer front seen in their Figure 6(c). Therefore, we cannot yet find any evidence in the literature that deviates from the behavior described above. Namely, that the CME and the wave are initially cospatial and decouple once the CME lateral expansion begin to decelerate. We will return to this discussion in Section 11.

Sometimes, the full EUV wave outline can be traced in both lateral and radial directions. One such example is the event on 17 January 2010 (Veronig *et al.*, 2010; Zhao *et al.*, 2011). The wave appeared as a dome surrounding the erupting CME (Figure 13). The dome was travelling faster in the radial ( $\approx 650 \text{ km s}^{-1}$ ) than in the lateral direction ( $\approx 280 \text{ km s}^{-1}$ ) which suggested that it may have been still driven by the CME in the radial direction whereas it

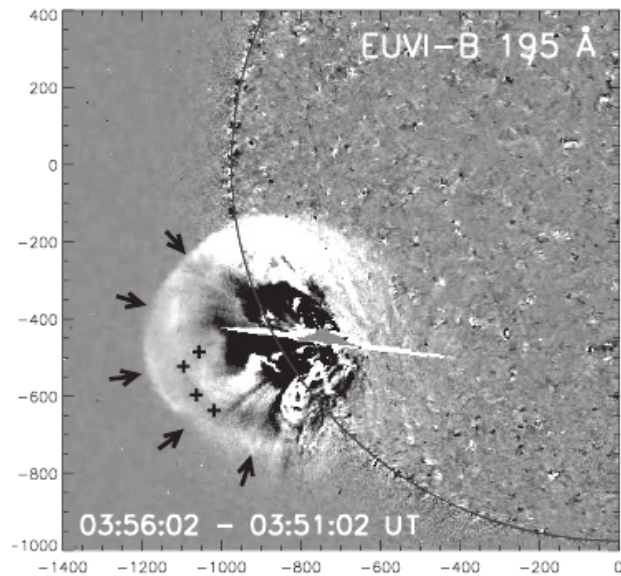


**Figure 13.** Observations of an EUV wave dome on 17 January 2010. The wave dome is marked by the arrows and the EUV CME by the crosses. From Veronig *et al.* (2010). Reproduced by permission of the AAS.

was freely-propagating in the lateral direction. The latter interpretation was further substantiated by the constant perturbation integral derived from the disk observations of the wave. However, the difference in the observed radial and lateral speeds could in principle result from different fast-mode speed profiles in the corresponding directions. Finally, Grechnev *et al.* (2011) reached essentially the same conclusion using a 3D blast wave model which was in a very good agreement with the ground tracks of the wave dome both on-disk and off-limb. Other examples of wave domes can be seen in the events of 13 June 2010, 7 June 2011 and 4 August 2011.

Estimates on the the maximum lateral expansion of CMEs in the lower corona can be derived from the recent AIA observations of the Kelvin-Helmholtz (KH) instability in two eruptions (e.g., Ofman and Thompson, 2011; Foullon *et al.*, 2011). This instability occurs at the interface of two fluids exhibiting velocity shear, see for example Tsinganos (1980). In the case of the AIA coronal observations, the two fluids are the structure of the erupting, and rotating, flux rope and the ambient, almost potential, coronal structures around the erupting flux rope. The instability manifests itself in the AIA movies as the development of rolls at the outer boundary of the erupting structure for an off-limb observation; rotating core dimmings could be its on-disk manifestation. The observations show that the KH rolls seem to be confined close to the erupting AR which implies that probably the lateral expansion of the CME in the lower corona has a similar scale.

The lateral extent of CMEs at the base of the corona can be also approximated by comparing estimates of the mass content in the core dimmings  $m_{dim}$  from

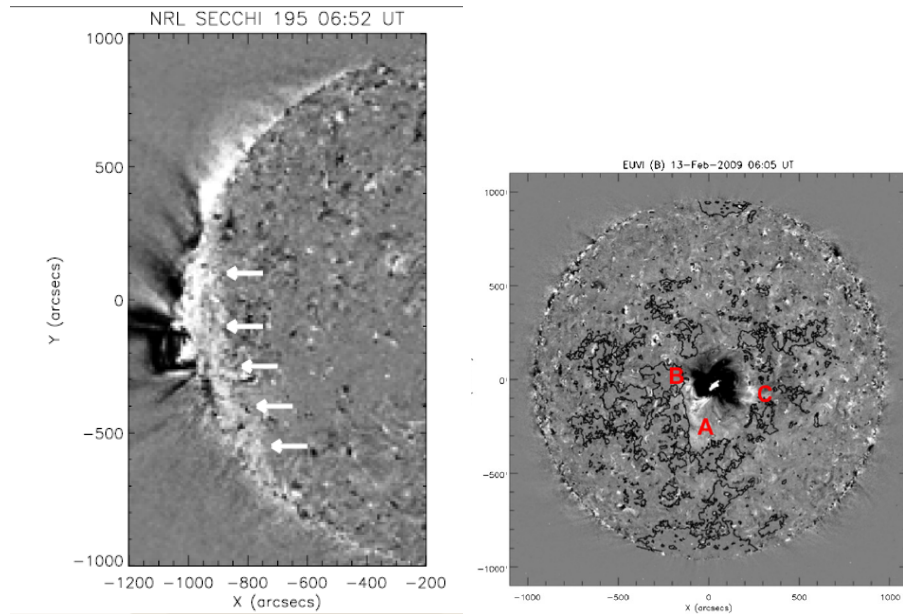


**Figure 14.** Examples of EUV waves exhibiting brightenings. Left panel from Attrill *et al.* (2007a) (25 January 2007 event) and right panel from Cohen *et al.* (2009) (13 February 2009 event). Right panel reproduced by permission of the AAS.

EUV observations and that of the associated CME,  $m_{CME}$  from WL coronagraph observations. Aschwanden *et al.* (2009) found that  $m_{dim}/m_{CME} = 1.1 \pm 0.2$  for a set of events observed by STEREO. Therefore, core dimmings can supply sufficient mass to match the WL CME masses. A corollary of these results is that only the core dimmings could be associated with mass evacuation. We could expect higher CME masses than observed if the low corona opened at scales exceeding the scale of core dimmings, as the pseudo-wave models suggest.

## 6. Brightenings, Secondary Dimmings and Volume Expansions

Observations of EUV waves revealed a series of features which strongly appeal to pseudo-wave interpretations (Attrill *et al.*, 2007a,b, 2009; Cohen *et al.*, 2009; Zhukov, Rodriguez, and de Patoul, 2009; Dai *et al.*, 2010; Schrijver *et al.*, 2011; Warmuth and Mann, 2011). These include stationary brightenings, large-scale secondary dimmings and erratic (including a series of accelerations and decelerations) or "slow" (i.e. below the coronal sound speed) kinematic profiles like these reported by Zhukov, Rodriguez, and de Patoul (2009) and Warmuth and Mann (2011) respectively (see the discussion in Section 2). Such a kinematic behavior cannot be reconciled with fast-mode waves which travel at either constant speed or decelerate and the speed is always  $\geq$  of the fast-mode speed.

Examples of brightenings associated with EUV waves are given in Figure 14 where several brightenings can be seen at locations on the EUV wave fronts for waves on 25 January 2007 and 13 February 2009. Such brightenings are seen

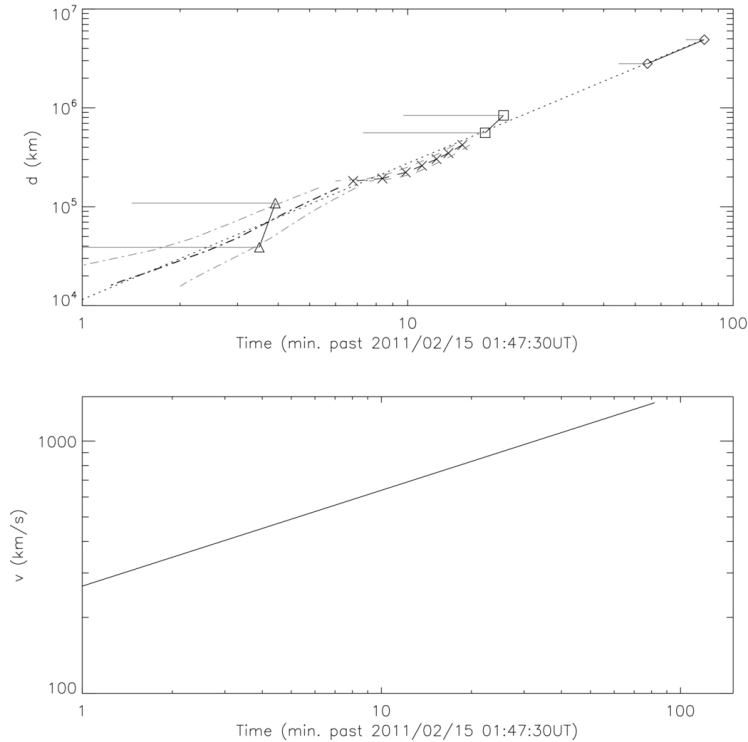


**Figure 15.** Observations of an EUV wave which take place on 15 February 2011. The upper panel contains the time-distance and the lower panel the speed-distance plot for several features observed in association with event. For radial displacements: STEREO-A/COR2 (diamonds), STEREO-A/COR1 (squares), STEREO-A/EUVI/195 (triangles). For on-disk displacements: expansion front for AIA 193 at the central meridian measured along a great circle through the central flare site (crosses), expansion feature traced in AIA 335, assuming a  $45^\circ$  inclination relative to the local horizontal direction of the tracked loops (dash-dotted line). From Schrijver *et al.* (2011). Reproduced by permission of the AAS.

at even higher temperatures with XRT (Golub *et al.*, 2007) on *Hinode* (Attrill *et al.*, 2009). The brightenings could result from magnetic reconnections between the erupting flux rope and ambient QS fields of favorable polarity. Note here that localized brightenings in association with EUV waves are not only seen in the EUV and SXR but also in  $H\alpha$  (Warmuth *et al.* 2004) and in He I 10830 Å (Vršnak *et al.*, 2002). These brightenings are seen slightly ahead of the EUV wave front.

Smooth volume expansions are another important indicator for pseudo-waves. The Schrijver *et al.* (2011) study tracked several features of the event: the fronts of expanding loops, a bright diffuse front, and the associated CME. They found a smooth transition between these features, and particularly between the expanding loops and the wave front (see the upper panel of Figure 15). The combined kinematics are consistent with acceleration (lower panel of Figure 15) which under certain conditions could be at odds with a fast-mode wave. However, fast mode waves can sometimes also manifest acceleration (see the discussion in Section 2). Current-density renderings from an MHD simulation

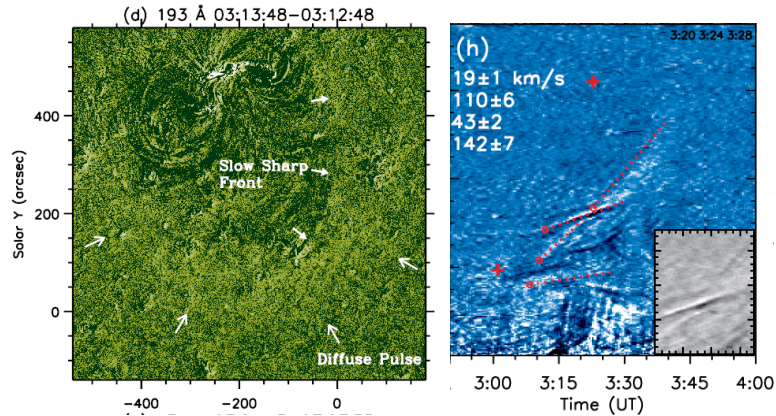


**Figure 16.** AIA observations of an EUV wave which took place on 3 April 2010. Left panel shows the double wave front and right panel shows multiple and crossing components in a time-distance plot at a given direction. From Liu *et al.* (2010). Reproduced by permission of the AAS.

of the expanding current shell around an erupting flux rope resulted in fronts similar in appearance to the observed wave fronts.

Besides the strong core dimmings, presumably mapping to the legs of the erupting flux rope, large-scale secondary dimmings trailing the EUV wave front can be seen by either conveniently scaling the images (e.g., Delannée and Aulanier, 1999) or in the perturbation profiles (e.g., Muhr *et al.*, 2011). These dimmings could result from the plasma evacuation behind the erupting flux rope, similarly to the stronger core dimmings, therefore justifying a pseudo-wave interpretation. However, plasma rarefaction in regions from where a compressive wave has passed could have a similar effect (e.g., Muhr *et al.*, 2011).

As discussed in the previous Sections, several of these events with evidence of non-wave components/interpretation have been analyzed by other groups, who found support for a wave interpretation based for example on wave kinematics, reflections, 3D structure etc. This however does not necessarily mean that these analyzes are mutually exclusive. We will return to this very important issue in Section 11.

## 7. Multiple components and ripples

The ultra-high cadence of AIA observations brought new information on the structure of EUV waves. The first observations of an EUV wave observed by AIA were reported by Liu *et al.* (2010). The wave took place on 3 April 2010 and was characterized by multiple components moving ahead of a set of erupting loops which presumably resulted into a CME. Besides the usual diffuse front associated with the global EUV wave, several sharper fronts were seen moving in its wake. While the diffuse front was moving at more or less a constant speed of  $\approx 200 \text{ km s}^{-1}$ , the two sharp fronts, a slow one at  $\approx 80 \text{ km s}^{-1}$  and a faster one at  $\approx 160 \text{ km s}^{-1}$ , were accelerating and even crossed each other (as seen in projection)

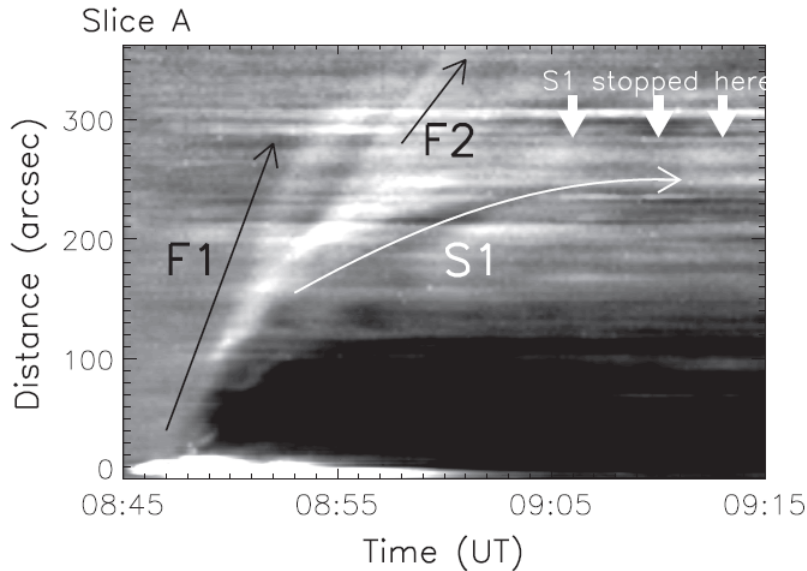


**Figure 17.** Distance-time plots of an EUV wave which took place on 27 July 2010 showing evidence of two components. From Chen and Wu (2011). Reproduced by permission of the AAS.

and then propagated independently (see Figure 16). The characteristics of the diffuse front (speed of the order of the fast-mode speed in the QS and almost isotropic propagation) seem consistent with a wave interpretation. On the other hand the sharp fronts can in principle result from compression ahead of the expanding loops. However, this interpretation has difficulty explaining why after the two fronts cross they generate another set of weaker fronts in the form of ripples. A possibility for these ripples is that they could be related to some sort of secondary waves as found by Li *et al.* (2012) (see Section 3), or that they are simply the result of oscillations of loops highly inclined towards the solar surface. Note here that TRACE (Handy *et al.*, 1999) made the first observations of multiple fronts associated with EUV waves (Wills-Davey and Thompson, 1999; Harra and Sterling, 2003). However, given the small field of view of TRACE it was not possible to tell how far these disturbances propagated.

Another example of an EUV wave exhibiting multiple fronts can be found in Chen and Wu (2011). This event on 27 July 2010 showed evidence for two fronts. A fast front traveling at  $470\text{--}560\text{ km s}^{-1}$  speeds, followed by a slower front traveling at  $170\text{--}190\text{ km s}^{-1}$  speeds (see Figure 17). The slower component decelerated and eventually seemed to "stop" at some distance from its origin. The stopping location seemed to coincide with the location of a magnetic field separatrix as deduced from a magnetic field extrapolation. Another example of multiple-fronts wave event is the 13 June 2010 event described in detail in Section 10 (see for example panel (c) of Figure 19).

These examples call for a hybrid interpretation of the observations. The outer front, is consistent with either a linear fast-mode wave at almost constant speed

---

(Liu *et al.*, 2010) or with a shocked fast-mode wave traveling at higher speeds (Chen and Wu, 2011). The second inner front(s) could correspond to pseudo-waves associated with the expanding loops of the eruption. The observed disk behavior seems consistent with off-limb observations of EUV waves showing two fronts which split at some point (e.g., Figure 12 and Section 11).

## 8. Spectroscopic Observations

Observations from the *Extreme Imaging Spectrometer* (EIS; Culhane *et al.* (2007)) on-board *Hinode* supplied new important constraints about EUV waves. EIS raster observations taken over dimming regions in the cores of the ARs which gave rise to EUV waves, showed significant blue-shifts and an increase in the non-thermal velocity (e.g., Harra *et al.*, 2007; Imada *et al.*, 2007; Asai *et al.*, 2008; Jin *et al.*, 2009; McIntosh, 2009; Attrill *et al.*, 2010; Chen, Ding, and Chen, 2010; Chen *et al.*, 2011; Dolla and Zhukov, 2011). The observed blue-shifts could be the signature of the radially and laterally expanding CME. At times, the magnitudes of the observed blue-shifts ( $< 50 \text{ km s}^{-1}$ ) are smaller than the “typical” propagation speeds of EUV waves across the solar surface ( $> 200 \text{ km s}^{-1}$ ) deduced from imaging instruments, which could be explained by the continuous inwards bending of the magnetic field caused by the erupting flux which decreases the line of sight component of the speed (Chen, Ding, and Chen, 2010).

We stress here that the above observations were taken at or near the source AR, and thus did not allow the study of the wave propagation sufficiently far from its source. The first observation of this kind was performed by Harra *et al.* (2011) for an event which took place on 16 February 2011. EIS was taking ‘sit-and-stare’ observations using a 512 arcsec long slit. The time-evolution of the Doppler-shift along the slit can be seen in Figure 18. Near the source AR (lower part of the slit) the “standard” blue-shifted pattern can be seen. A couple of outward propagating red-shifted ridges can be seen away from the source AR. The average speed of the ridges is  $\approx 500 \text{ km s}^{-1}$  which is similar to the speed of the associated EUV wave observed by AIA. The red-shifts could be signatures of plasma pushed downwards and compressed by a coronal MHD shock, similar to the Uchida (1968) picture for chromospheric Moreton waves. In a follow-up study of the same event, density sensitive line ratios of two Fe XIII lines revealed density changes during the wave transit along the EIS slit which were however within the noise level Veronig *et al.* (2011). This supplies a spectroscopic demonstration of the small density changes normally associated with EUV waves. Moreover, Veronig *et al.* (2011) found negligible mass motions in a He II line, suggesting that the wave was not strong enough to perturb the underlying chromosphere. This observation is broadly consistent with the double-front observations discussed in the previous Section.

Spectroscopic observations could be also used to get coronal seismology information of the background corona where EUV waves are propagating. West *et al.* (2011) used EIS density sensitive lines to get the coronal density over the QS where the 13 February 2009 wave propagated. From the propagation speed

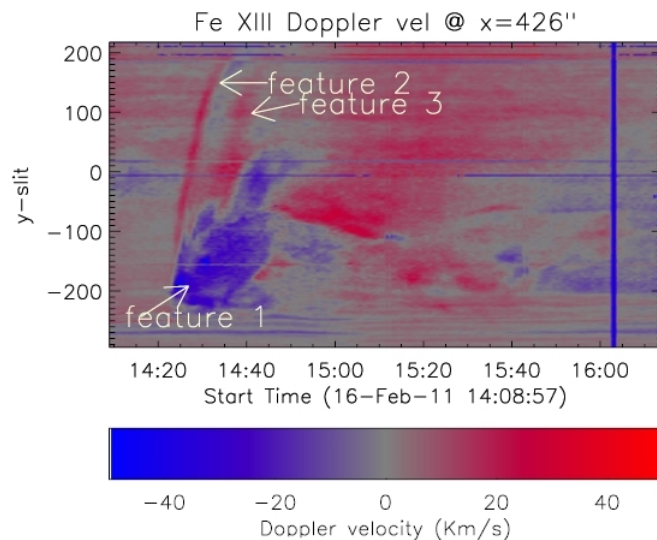


**Figure 18.** Spectroscopic observations of an EUV wave on 16 February 2011. Time-distance plot of the Doppler shifts in a Fe XIII line observed by EIS/Hinode. From Harra *et al.* (2011). Reproduced by permission of the AAS.

of the wave, the inferred density, and under the assumption that the observed disturbance was a fast-mode wave they obtained  $0.7 \pm 0.7$  G for the magnetic field.

## 9. Energetics

Given the observationally-deduced physical parameters of EUV waves it is worthwhile to make some estimates of their energy content. This is particularly important for assessing their overall role in the energy budget of energetic phenomena like flares and CMEs which are associated with and occur in tandem with EUV waves.

The kinetic energy flux  $F_{kin}$  can be written as:

$$F_{kin} = \rho(\delta v)^2 v_{gr}/2, \quad (1)$$

with  $\rho$  the mass density,  $v_{gr}$  the group speed and  $\delta v$  the velocity perturbation. For weak (linear) perturbations a lower limit for  $F_{kin}$  is (e.g., Liu *et al.*, 2011),

$$F_{kin} = \rho(\delta I/I)^2 v_{gr}^3/8, \quad (2)$$

with  $\delta I/I$  the relative intensity change. It is assumed that the temperature does not change and therefore it is  $I \propto n^2$ . Taking typical values for  $v_{gr}=300$  km s<sup>-1</sup>,  $\delta I/I=1.15$  and for a QS coronal density of  $5 \times 10^8$  cm<sup>-3</sup> we find  $F_{kin} = 1.9 \times 10^3$  erg cm<sup>-2</sup> s<sup>-1</sup>.



---

The radiative losses flux  $F_{rad}$  is given by:

$$F_{rad} = n^2 L \Lambda(T), \quad (3)$$

with  $n$  the electron density,  $\Lambda(T)$  the temperature dependent radiative losses function, and  $L$  is a characteristic lengthscale where the bulk of the observed emission comes from. We assume that  $L$  does not substantially change during the propagation of EUV waves; moreover the temperature is kept constant. The latter assumption leads probably to an overestimate of  $F_{rad}$  given that  $\Lambda(T)$  is generally a decreasing function of  $T$  in coronal temperatures and sometimes there is a small temperature increase associated with EUV waves as discussed in Section 4. For a 10 % increase in the density  $F_{rad}$  increases by 21 % with respect to the pre-wave conditions. Using the standard QS coronal radiative losses flux from Withbroe and Noyes (1977) we get  $F_{rad} = 1.2 \times 10^5 \text{ erg cm}^{-2} \text{ s}^{-1}$ .

For coronal thermal conduction flux  $F_{cond}$  it is:

$$F_{cond} \propto T^{7/2} / L^2. \quad (4)$$

For a temperature increase of 7 % (Schrijver *et al.*, 2011) we have a 26 % increase in  $F_{cond}$ . Using the standard QS coronal thermal conduction flux from Withbroe and Noyes (1977) we get  $F_{cond} = 2.5 \times 10^5 \text{ erg cm}^{-2} \text{ s}^{-1}$ .

The kinetic energy flux is rather small compared to the various QS energy terms, it can become sizeable only for ultra-high speeds (Equation 2, for example the  $2000 \text{ km s}^{-1}$  disturbance described in Liu *et al.* (2011)). On the other hand, the radiative and conductive fluxes represent small, yet sizeable increases over the ambient QS corresponding values.

We can now calculate a proxy for the total energy  $E_{wave}$  associated with EUV waves:

$$E_{wave} = (F_{kin} + \Delta F_{rad} + \Delta F_{cond}) 2\pi R dR \Delta t, \quad (5)$$

with the  $\Delta$  quantities representing the change in the corresponding fluxes associated with the EUV wave (i.e., the fluxes calculated from Equations 3 and 4) with respect to the standard energy losses in terms of radiation and thermal conduction of the QS corona (Withbroe and Noyes, 1977). We assume that the wave is a spherical shell of radius  $R$  and thickness  $dR$  and  $\Delta t$  is its life-time. Using standard values for  $R = 300 \text{ Mm}$ ,  $dR = 50 \text{ Mm}$  and  $\Delta t = 40 \text{ min}$  we finally find that  $E_{wave} = 1.8 \times 10^{29} \text{ erg}$ . The resulting energy is relatively substantial; it is the energy of a small flare and lies in the low-end of the CME energy distribution (Vourlidas *et al.*, 2010). This may not be unexpected: even though EUV waves do not significantly perturb the ambient corona they may however correspond to significant amounts of energy given they are global phenomena. We caution here the reader that our energy calculations have to be seen as crude order of magnitude estimates.

## 10. The genesis of EUV waves

As discussed in the Introduction, EUV waves are associated more with CMEs than flares. This is true from the observational as well as from the theoretical

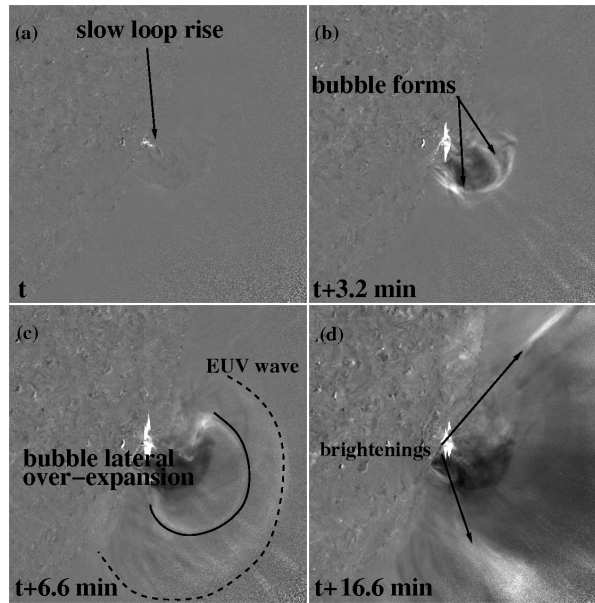


**Figure 19.** Evolutionary pattern towards the formation and during the EUV wave of the 13 June 2010. Base-ratio images are shown. Slow loop rise from the active region core (panel a) leads to the formation of a bubble (i.e. EUV cavity; panel b). The bubble experiences a short period of lateral over-expansion which sets a wave around it (panel c). Two quasi-stationary brightenings form at locations where the bubble reaches maximum lateral extent (panel d).

point of view. Indeed, most theoretical ideas, whether wave or pseudo-wave driven, rely upon the CME as either the wave driver or as the wave itself. High cadence movies of EUV waves observed either on disk or off-limb show that the first instances of a wave front are seen ahead of the flanks of the rising and expanding loops of the early CME (e.g., Long *et al.*, 2008; Patsourakos *et al.*, 2009; Kienreich, Temmer, and Veronig, 2009; Patsourakos and Vourlidas, 2009; Patsourakos, Vourlidas, and Kliem, 2010; Patsourakos, Vourlidas, and Stenborg, 2010; Veronig *et al.*, 2010; Liu *et al.*, 2010; Ma *et al.*, 2011; Kozarev *et al.*, 2011; Schrijver *et al.*, 2011). Disk observations of Moreton waves show a similar trend with the first wave fronts seen in the AR periphery and never in its core (e.g., Balasubramaniam *et al.*, 2010; Temmer *et al.*, 2009; Muhr *et al.*, 2010).

Based on off-limb STEREO and AIA observations of impulsive events (e.g., Patsourakos, Vourlidas, and Kliem, 2010; Patsourakos, Vourlidas, and Stenborg, 2010; Kozarev *et al.*, 2011; Ma *et al.*, 2011; Cheng *et al.*, 2012), the following evolutionary pattern is seen (Figure 19 and 21). A set of loops is slowly rising in the core of the source AR region (Figure 19(a)); these loops progressively start to map on the edges of a bubble (Figure 19(b)), which eventually evolves into (at least partially) the WL CME observed later with coronagraphs. The bubble undergoes a period of strong lateral expansion which launches the EUV wave at the flanks of the bubble; sometimes the full wave dome becomes visible (Figure 19(c)). While the bubble reaches a more or less constant lateral extent, the detached wave propagates further away. The above pattern is common among

---

impulsive events associated with EUV waves. We have been able to gather the following partial list: 3 June 2007, 2 January 2008, 25 March 2008, 13 February 2009, 16 December 2009, 17 January 2010, 3 November 2010, 11 February 2011, 15 February 2011, 24 February 2011, and 8 March 2011. Note that entire stages in this evolutionary pattern would have been poorly resolved or even entirely missed without the high cadence of the EUVI and AIA instruments.

The expansion of the bubble in the radial and lateral directions can be quantified by measuring its aspect ratio, defined as  $\text{height}(t)/\text{radius}(t)$  of the best-fit circle or sphere to the bubble. The aspect ratio is decreasing for a short-period which signifies that the bubble undergoes a period of *inflation* or *lateral over-expansion*, i.e. it grows faster in the lateral than in the radial direction, as was first discussed in Patsourakos, Vourlidas, and Kliem (2010) and Patsourakos, Vourlidas, and Stenborg (2010). This period of lateral inflation marks the launch of an EUV wave. The lateral over-expansion could be driven by the high magnetic pressure within the bubble as it tries to reach equilibrium with the low pressure of the ambient QS fields. Ideal (expansion of flux surfaces around rising flux ropes with decreasing flux rope current) and non-ideal (reconnection adding new flux to the erupting flux rope) MHD effects can also account for the lateral over-expansion (Kliem et al. 2012, in preparation). The start of this inflationary period roughly marks the launch of the wave in their simulations. The simulation results provide further support to the idea that the expanding CME flanks are the trigger of the wave.

As a quantitative test for this possibility we applied the piston-driven model of large-scale coronal waves of Temmer *et al.* (2009). This model essentially predicts the ground tracks of large-scale coronal disturbances given the kinematics of the driver (the temporal evolution of its radius  $r(t)$  and height  $h(t)$ , for example) as well as the value of the (uniform) Alfvén speed ( $V_A$ ). Moreover, the model specifies the amplitude of the disturbance  $f(d)$  as an exponential function for example, i.e.,  $f(d) = e^{-d/p}$ , with  $d$  the distance from the initial position of the driver and  $p$  a scale-distance of the disturbance.

For the 13 June 2010 event, the bubble fitting supplied the kinematics of the possible wave driver ( $h(t)$  and  $r(t)$ ) Patsourakos, Vourlidas, and Stenborg (2010). From a polar off-limb map of the event a  $p$  of  $\approx 0.12 R_\odot$  was deduced from the intensity distribution of the wave at a height of  $0.17 R_\odot$ , which is similar to the emission (formation) heights of EUV waves discussed in Section 5. Several points along the wave were manually extracted from that map. Therefore, the observations almost fully constrained the Temmer *et al.* (2009) model with the exception of  $V_A$ . Note that Temmer *et al.* (2009) were not able to reproduce the ground tracks of a Moreton wave which took place on 17 January 2005 using the model above with the associated CME time-height measurements. They proposed that either the CME flanks or the flare blast wave generated the Moreton wave.

Figure 20 contains the predicted ground tracks of the large-scale disturbance using the observed  $h(t)$ ,  $r(t)$ , and  $d$  for different values of  $V_A$ . A very good agreement between the predicted ground track and few selected points along the wave is achieved for  $V_A=400 \text{ km s}^{-1}$ . This value for  $V_A$  in the low solar corona is more appropriate to QS rather to ARs where it can reach speeds exceeding

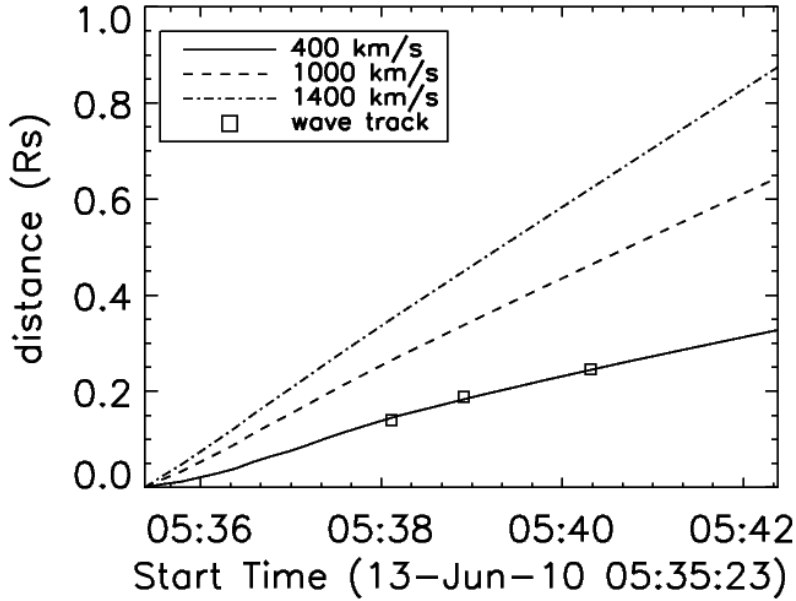


**Figure 20.** Predicted ground track of a coronal wave using the Temmer *et al.* (2009) model. Inputs were the EUV bubble kinematics (time evolution of height and radius) of the EUV wave which took place on 13 June 2010. The tracks correspond to an Alfvén speed of 400  $\text{km s}^{-1}$  (solid line), 1000  $\text{km s}^{-1}$  (long dashes) and 1400  $\text{km s}^{-1}$  (dash-dot); the boxes correspond to the observed off-limb ground track of the wave at a height of  $0.17 R_{\odot}$ .

$1000 \text{ km s}^{-1}$ . It is thus plausible that the wave trigger were the flanks of the bubble which expanded over QS regions rather than its front which expanded in a higher Alfvén speed environment. MHD simulations show evidence of propagating disturbances at the flanks of erupting flux ropes (e.g., Chen *et al.*, 2002; Pomoell, Vainio, and Kissmann, 2008; Kliem *et al.*, 2012, in preparation). Further observational studies of over-expanding bubbles are required.

## 11. Towards a Coherent Picture of EUV waves

EUV waves represent an excellent example of scientific endeavour. A serendipitous discovery opens up a new area of solar physics research, leads to controversy over its interpretation and eventually reaches closure. Thanks to a string of new missions and instruments over the last decade, we are getting closer to the last stage—understanding EUV waves and their relation to the explosive energy release in the Sun. The observations from multiple viewpoints have played (and will continue to play) a particularly important role in clarifying the nature of EUV waves. We believe that, by synthesizing the existing results, we can offer a unified picture of EUV wave signatures which effectively removes most of the wave versus pseudo-wave controversy. This picture builds upon previous work which considered the *hybrid* nature of EUV waves (see the discussion in

---

Introduction). Before we discuss this picture, it is useful to briefly recap the most important findings from the recent observations. In the following list, we mark each item with a *W* and/or *P-W* to show whether it is consistent with a wave or a pseudo-wave interpretation, respectively. Table 1 contains a summary of some properties of EUV waves.

- Despite a large range of initial speeds, all EUV waves decelerate to a narrow range of  $\sim 200\text{-}300 \text{ km s}^{-1}$  which corresponds to the nominal fast-mode speed in the quiet Sun (*W*).
- Observations of wave reflection and transmission at coronal hole boundaries (*W*).
- Observations of decelerations or complete disappearances in ARs (*W*).
- EUV wave and CME kinematics differ (*W*).
- Temporary dimmings (*W*).
- Long-term dimmings (*P-W*).
- Brightenings at the wave front and its wake (*P-W*).
- Multiple wave fronts travelling at different speeds. Sometimes they cross each other and produce secondary ripples (*W* and *P-W*).

The observations (and MHD modeling) suggest that global EUV waves are more consistent with a (fast-mode) wave interpretation. This is rather expected since any kinetic disturbance will launch waves in a magnetized plasma. It is not surprising, therefore, that the fast-mode wave was the initial interpretation put forth soon after the discovery of this phenomenon (Thompson *et al.*, 1998, 1999). Then, why does the controversy over the nature of the EUV waves persist? Why are there cases where different observers reach opposite conclusions from the analysis of the very same events?

We believe that the answers to these questions lie in a sort of 'structure confusion'. EUV waves, being associated with CMEs, occur in tandem with an extensive 'zoo' of other phenomena (e.g., core and extended dimmings, stationary brightenings, deflections and oscillations, multiple fronts and ripples, flows, etc). All these phenomena evolve in time and size and hence can be associated, or rather confused, with the wave. The confusion can be avoided if the definition of the EUV wave is kept in mind. In other words, the EUV wave is *the outermost propagating intensity front reaching global scales*. Most of these phenomena extend, at best, to nearby ARs or coronal holes. It is therefore important to carefully trace the proper front (the outermost one) amidst the multitude of all the other structures and time-evolving phenomena. In that case, combinations of disk and off-limb observations as well as full-sphere viewing and high cadence can prove invaluable.

The next step, is to realize that the terms 'EUV wave' and 'CME' are not equivalent. In our experience, this is the main source of confusion regarding the EUV wave nature in the literature. Sometimes the 'EUV wave' is singled out while discussing the CME front or vice versa. Other times attempts are made to connect white light fronts observed with coronagraphs to fronts observed with EUV instruments but not at the same height and finally other times there are "jumps" from wave to CME front as an event is followed in time. The root of the problem seems to be the imprecise definitions used sometimes for these terms.

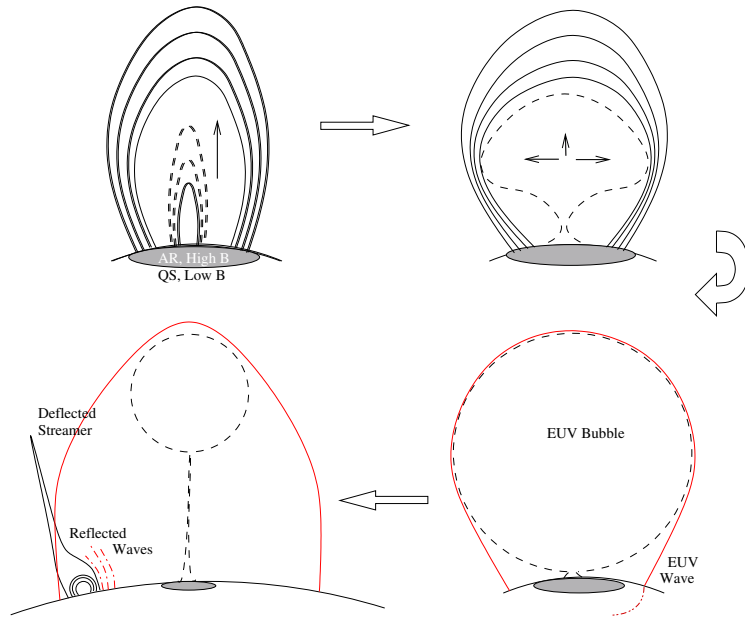


**Figure 21.** Schematic evolution of the genesis of a CME and its associated EUV wave. The cartoon represents a top-level synthesis of EUV wave observations as discussed and interpreted in this review. Top left: A set of outward expanding loops in the core of an active region (grey area) always occur before a CME-EUV wave eruption. Top right: At some point, the loops disappear and give rise to an expanding bubble. The bubble undergoes a very short period of *fast lateral expansion* compressing the surrounding field as it expands. Bottom right: The bubble eventually reaches its maximum lateral extent in the low corona and grows self-similarly from that point on. The fast expansion drives a wave around the edge of the EUV bubble. The wave forms when the lateral expansion enters the low magnetic field of the Quiet Sun (where the fast mode speed is lower than in the AR). The wave is driven at this stage with potentially a very small standoff distance. The wave *decouples* from the CME when the lateral expansion speed drops. Bottom left: At a later stage, the CME is moving out in the corona, possibly driving a shock around it. The original EUV wave is propagating at larger distances reflecting off and/or propagating through ARs or coronal holes, and causing deflections and oscillations in EUV loops. It may be no longer driven. See Figure 19 for an actual observation that corresponds closely to this scenario.

As part of our synthesis effort, we propose a set of definitions here: an EUV wave is a disturbance propagating along the EUV coronal surface at large distances from an eruption. A CME is a magnetic disturbance (i.e. a magnetic fluxrope) propagating outwards from the corona.

The strong association of EUV waves to CMEs implies that an *expanding driver* is likely following the expanding EUV wave (Figure 21). Both structures will appear as a wave front in the images but their behavior (and interpretation) will be different. For example and from the discussion of Section 2, the wave will propagate at the local fast-mode speed when it is in the linear regime or close to it and above it when it is in the non-linear regime while the CME can propagate at any speed. The wave will propagate to  $> 60^\circ$  from the erupting region while the CME flanks will stop at a coronal hole boundary or within  $30^\circ - 40^\circ$  since the average width of CMEs is  $\sim 60^\circ$  (St. Cyr *et al.*, 2000; Yashiro *et al.*, 2004).

---

By taking into account the dual nature of EUV wave/CME, most of the controversy over the nature of EUV waves can be removed. For example, for events showing evidence of two wavefronts (e.g. Figures 16, 17, 19), the inner brighter front is the expanding CME loops or bubble (and hence the *pseudo-wave*). The outer fainter front is the fast-mode wave (and hence the *wave*). The wave can be driven or freely-propagating depending on the stage of the CME evolution. These events are characterized by the existence of an EUV bubble or of a well-formed white light CME fluxrope (Patsourakos and Vourlidas, 2009; Patsourakos, Vourlidas, and Kliem, 2010; Liu *et al.*, 2010; Veronig *et al.*, 2010; Kozarev *et al.*, 2011).

Other events lack a well-defined CME structure in the EUV corona. But the CME is there and it will cause 'pseudo-wave'-like signatures. These are the cases that lead to opposite interpretations of the same data when the event is analyzed partially. An example could be the 15 February 2011 event. The relatively smooth transition among the height-time plots of the EUV wave, loops and white light CME reported in Figure 15 does not imply that the EUV wave and the CME front are the same (and hence that the EUV wave is a pseudo-wave as suggested by Schrijver *et al.* (2011)) but simply that the EUV wave and the CME front are *at the same location*. Without a clear manifestation of a CME front in the EUV it is hard to discount the latter interpretation. However, the reported volume expansions have, at some point, launched the "true" EUV wave undergoing reflections/transmissions as shown in Olmedo *et al.* (2012).

Distant brightenings are commonly discussed in such events in support of a pseudo-wave interpretation. Their explanation in terms of the CME driver is rather straightforward. When the erupting flux reaches its maximum lateral extension in the low corona it can generate features pertinent to pseudo-waves like stationary or moving brightenings. For example, strong brightenings at the sides of the erupting flux can be easily discerned from a side view (panel (d) of Figure 19). These are formed when the erupting flux "stops" at those locations (coronal hole boundaries) and ambient plasma is compressed and maybe heated. Given the inclination of these compressed structures, a disk observation of such an event would give the impression of moving brightenings<sup>1</sup>. A similar situation could have occurred, as discussed before, in the event analyzed by Chen and Wu (2011), see Figure 17, where a stationary brightening forms where the inner wave front seems to "stop".

We therefore propose that the majority of the observations can be reconciled by properly considering the spatial and temporal evolution of the CME vis-à-vis the expanding EUV wave. Figure 21 is our attempt to provide a unified picture of the CME-EUV wave coupling. It is a simplified cartoon which emphasizes the most important, top-level characteristics of the eruption but it can still account for the various observations of waves (or pseudo-waves). Figure 19 is the closest observational example we could find. In this picture, the EUV wave is driven by an expanding CME. The wave appears if or when the speed of the CME expansion overtakes the local fast-mode speed. This happens more easily at the

---

<sup>1</sup>STEREO A observations with a disk view of this event did not have enough cadence to capture these features.

---

flanks since they encounter QS conditions (and hence lower fast-mode speeds) sooner than the radially outward moving CME parts. The wave front will tend to be very close to the CME front (small standoff distance) for fast accelerating CMEs. The two will separate when the CME either slows down or the wave encounters a lower fast-mode speed environment. There is no guarantee that an EUV front will form at the CME nose if (or while) the CME propagates inside a streamer because of its high plasma  $\beta$ . This implies that connecting a white light front to an EUV front must be done very carefully. As far as we can tell, this picture explains all of the available observations of EUV waves and contains both the wave and pseudo-wave interpretations.

Furthermore, this picture is strongly supported by MHD modeling. The recent advances in global MHD modeling of EUV waves recover many of the observed signatures (Linker *et al.*, 2008; Lionello, Linker, and Mikić, 2009; Cohen *et al.*, 2009; Schmidt and Ofman, 2010; Downs *et al.*, 2011). These models have the ability to generate realistic synthetic images of the global solar corona before and during EUV waves. This is achieved by solving consistently the field-aligned energy transport and using realistic boundary conditions. The waves are usually driven by the eruption of a postulated flux rope or by simply launching a velocity pulse. Several features seen in the observations like bubbles, multiple fronts, reflections *etc* can be seen in these simulations. As an example Figure 22 shows results from a recent study of the 25 March 2008 event (Downs *et al.*, 2011). The simulated EUV images of the left panel of this figure reproduce the bubble-like structure and propagating intensity fronts. They have similarities with actual observations shown in, for example, Figures 11 and 13. The right panel of Figure 22 shows time-distance plots of simulated emission measure along a track along the wave path. Two lanes can be seen, which resembles plots with similar format for observed events (e.g., Figure 17).

We note here that our picture may not be able to explain every nuanced structure associated with EUV waves (e.g., see the crossing ripples in Figure 16 and the possible explanations discussed in Section 7). But one needs to keep in mind that EUV waves do not have to be related to all observational features seen during explosive events. Therefore, the latter should not be included in the interpretations of such phenomena. This becomes evident in the most dramatic way with the ultra-high cadence and high sensitivity AIA movies where the entire corona seems to be in a stage of seamless agitation at any time including when EUV waves take place. An example of non-related features during EUV waves is narrow angular extent intermittent flows firing from the core of the source ARs *after* the early CME is underway. These are probably triggered by the general reconfiguration of the coronal magnetic field during a CME but have nothing to do with the wave itself.

## 12. Future areas of work

We have tried to present the large amount of recently published work on EUV waves and to suggest a simple scenario for their genesis which reconcile the sometimes conflicting interpretations of their observations. In our view, the



**Table 1.** Properties of global EUV waves compiled from recent observations.

average speeds ( km s <sup>-1</sup> )	200-400
initial speeds ( km s <sup>-1</sup> )	223-750
final speeds ( km s <sup>-1</sup> )	180-380
maximum distance from source (Mm)	350-850
width (Mm)	20-250
acceleration ( m s <sup>-2</sup> )	2.0×10 <sup>3</sup> - 150
magnetosonic-Mach number	1.08-1.4
intensity increase ( $I/I_0$ )	1.02-1.7
maximum temperature (MK)	2.8
maximum density increase	1.009-1.3
emission heights	50-100 Mm
3D shape	≈ spherical
relationship with CME	co-spatial (early), ahead (later)
kinetic energy flux ( erg cm <sup>-2</sup> s <sup>-1</sup> )	1.9×10 <sup>3</sup>
radiative losses flux ( erg cm <sup>-2</sup> s <sup>-1</sup> )	1.2 × 10 <sup>5</sup>
thermal conduction flux ( erg cm <sup>-2</sup> s <sup>-1</sup> )	2.5 × 10 <sup>5</sup>

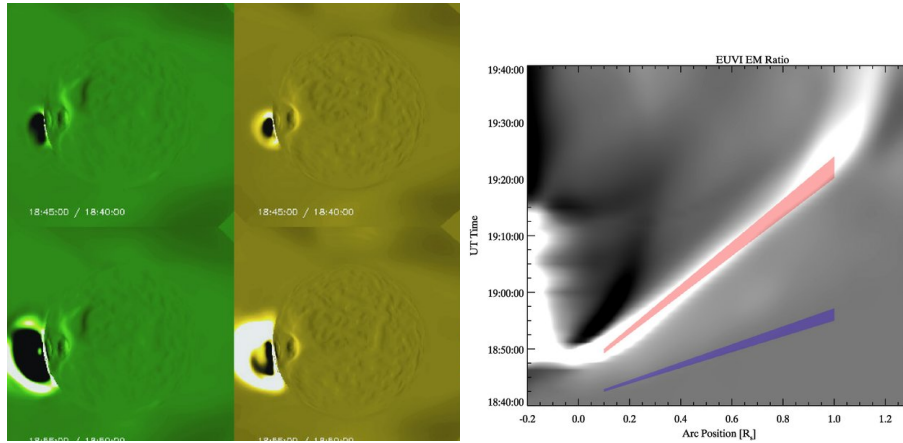


**Figure 22.** Global MHD simulations of an EUV wave which took place on 25 March 2008. Left panel: a series of synthetic base-difference images for the 195 (green) and 284 (yellow) EUVI channels. Right panel: time-distance plot of emission measure along a sector. From Downs *et al.* (2011). Reproduced by permission of the AAS.

community is not far from the resolution of the nature of EUV waves. However, important questions remain unanswered. Research will benefit greatly from the availability of high cadence observations from AIA and the full-Sun coverage afforded by the combination of AIA and EUVI-A and -B since mid-2011. We discuss below a list of such open questions.

1. *What determines the generation of a true wave?* We strongly suspect that the *impulsiveness* of the early CME evolution is the key parameter. Theoretical studies show that the driver needs to accelerate in a matter of few minutes to launch a large-scale wave or a shock with pulse amplitudes sufficient for

---

detection (e.g., Žic *et al.*, 2008; Pomoell, Vainio, and Kissmann, 2008; Downs *et al.*, 2011). The peak speed seems not to be the main factor, as long as it exceeds (at some point) the characteristic speed of the ambient medium. We have observed EUV waves in association with relatively slow drivers; e.g., the 13 February 2009 event with a radial speed of around  $200 \text{ km s}^{-1}$  (c.f. Figure 12) and the 13 June 2010 event with a peak speed of  $400 \text{ km s}^{-1}$  and rapid deceleration. The similarity in both events is the sharply peaked acceleration profile. Events with similar speeds but with more gradual acceleration profiles are not prone to generate visible EUV waves. The lack of observable wave signatures does not necessarily mean lack of waves. All motions in a plasma will drive some sort of a wave disturbance. However, gradually accelerating drivers will tend to create lower amplitude pulses farther away from the eruptions site. Hence, the associated wave density enhancements will be weaker and may escape detection. Deflections of distant (from the eruption site) structures are as common in EUV images as they are in coronagraph images. The corollary, for gradually accelerating events, is that any propagating EUV signatures will be associated with the expanding CME (the pseudo-wave) and will be likely restricted to long-term dimmings in the vicinity of the eruption.

We have suggested in the past, and discussed in Sections 10 and 11, that the strong lateral expansion is the key factor for the wave generation. Therefore, the determination of the duration and the lengthscale of the driver acceleration in both the radial and lateral direction for several EUV wave events should be an important task for the future.

2. *Determine when and where pseudo-wave and wave decouple.* The ambient environment is probably a significant player in this question. In Section 10, we discussed how the expanding CME bubble, and more precisely its flanks, launch an EUV wave. The flanks, as they encounter weak QS fields, will strongly expand. The expansion will happen closer to the source AR, and occur over a larger area, when the AR is surrounded by mainly QS areas, which is the case during solar minimum conditions. However, as the cycle peaks, nearby ARs and equatorial coronal holes may prevent the strong lateral expansion of the CME bubble or the formation of a large scale wave. In this case, we expect that the volume expansion of the bubble, i.e. the pseudo-wave, would dominate the wave signatures until the true wave forms further away (assuming a sufficiently energetic event). Therefore, EUV waves taking place during solar maximum conditions could have more pronounced CME (pseudo-wave) signatures.
3. *Establish the exact relationship between type-II metric shocks and EUV waves.* Statistical studies show a rather high degree of correlation between metric type-IIs and EUV waves. Biesecker *et al.* (2002) showed that metric type-IIs occurred in tandem with at least 69% of EIT waves and Klassen *et al.* (2000) found an even higher degree of correlation (almost 90%). Warmuth *et al.* (2004) found a 100% correlation between type-IIs and Moreton waves. Finally, radioheliographic observations show that the sources of type II burst are generally consistent with coronal wave signatures (e.g., Pohjolainen *et al.*, 2001; Khan and Aurass, 2002; Vršnak *et al.*, 2006).

---

Even though the existence of a close association between metric type-IIs and EUV waves is well established some of the details are missing. Metric type-IIs generally last from three to ten minutes while the EIT cadence is 12 minutes or so. The scarcity of metric type-IIs during the extended minimum prevented any good comparisons with EUV observations but the situation has changed in the last years. Kozarev *et al.* (2011) and Ma *et al.* (2011) presented detailed comparisons of EUV wave and metric type-II kinematics showing a close correspondence between the two for the 13 June 2010 event; namely, the start of the radio emission start and the EUV wave appearance coincide to within less than a minute. They estimate the origin of the radio emission at the nose of the outgoing CME/wave. The joint analysis of the band-splitting of the radio dynamic spectrum and the stand-off distance between the shock driver (bubble) and the shock from the EUV observations of this event allowed to infer some estimates of the magnetic field at the base of the corona ( $\approx 1.3 - 1.5$  G, Gopalswamy *et al.*, 2012). A study of several more events by Vourlidas, Patsourakos, and Kouloumvakos (2011) suggests that the radio emission appears at, or near, the peak of the CME acceleration profile when an EUV wave also forms. In most cases, the EUV wave is visible only at the flanks of the CME, so these authors proposed that the radio emission originates at the flanks of the outgoing CME, in agreement with past imaging results from metric type-IIs (Gary *et al.*, 1984). It seems, therefore, that the radio observations provide strong support for the wave nature of EUV waves but the origin of the metric type-II emission (front or flanks) remains unclear. This is an important area of research for the future.

4. *How frequent are EUV wave reflections?* We saw in Section 3 that sometimes EUV waves seem to reflect at or even to go through coronal holes and ARs. This is the expected behavior and should be common, if EUV waves are true waves. But to firmly establish this, we need to expand from individual event to statistical studies. Perturbation-profiles analysis can be used to test if energy is roughly conserved between the incoming and the reflected and transmitted waves.
5. *3D relationship between EUV waves and CMEs.* A limiting factor in studies relating EUV waves and CMEs in 3D of Section 5 is that they are dealing with slow associated CMEs. As a result, when the CME emerges into COR1 field of view the EUV wave is weak and diffuse. It is thus desirable to perform this type of CME-EUV wave modeling/comparison for EUV waves which are associated with fast CMEs. This will allow the CME to emerge early enough into the coronagraph field of view when the wave is still strong. PROBA-II/SWAP (Berghmans *et al.*, 2006) off-point EUV images which can follow the early EUV CME at much larger heights than any current EUV imager, up to  $1 R_{\odot}$  above the solar limb, can also help into the wave-CME comparisons.
6. *What is the energy budget of EUV waves?* In Section 9 we made some order of magnitude estimates of the energy content of a 'typical' EUV wave. It is highly desirable to perform detailed calculations of the various energy terms for specific EUV wave events as a function of time and then deduce the total energy shed into each wave event. The wave energy could be compared with the corresponding energies of the associated CMEs and flares to determine the

---

energy partition. AIA multi-channel coronal observations can supply DEMs at each point across and during EUV waves which can be then used to determine the corresponding radiative losses.

7. *Establish possible links between Solar-Energetic-Particles (SEP) events and EUV waves.* Recent work by Rouillard *et al.* (2011) and Rouillard *et al.* (2012) (submitted) combine the 360-degree coverage of EUVI with AIA wave observations and shows that the lateral extensions of strong (i.e., associated with shocks) EUV waves could provide reliable estimates on the angular extensions, injection times, and intensities and of associated SEP events at the coronal base. Such work supply important clues on the origins of accelerated particles in SEP events (i.e. low *vs.* outer corona origins).
8. *What is the role of flares as drivers of EUV waves?* The strong increase in plasma pressure associated with flares is capable of launching a blast-wave. While it seems as if flares are quite unlikely to drive global EUV waves (see the discussion in the Introduction) they may be a wave-driver under some special conditions. The key here may be the spatial location of the flare. If the flare occurs at or close to the AR core, the very strong vertical gradients in the fast-mode speed would strongly refract the wave upwards with little lateral expansion (Wang, 2000; Patsourakos *et al.*, 2009). On the other hand, waves launched with some offset from the AR core would expand more easily in the lateral direction and therefore give rise to a global EUV wave. Moreover, calculations of the volume expansions of flare heated loops showed that they can drive large-scale waves and shocks if the flare occurs away from regions of very low magnetic  $\beta$  (i.e. AR cores, Vršnak and Cliver, 2008). Another important parameter is the timing between the flare and wave-onset. For example Muhr *et al.* (2010), Patsourakos *et al.* (2009) and Veronig, Temmer, and Vršnak (2008) found that the associated flares peaks occur before the wave onsets thus invalidating a flare driver. Therefore, statistical studies of the flare locations, for particularly wave events without an associated eruption, and of the relative flare-wave timings are required.
9. *Establish the relationship between Moreton waves and EUV waves.* Previous studies showed that if Moreton waves are the chromospheric counterparts of coronal waves observed with EIT, then the latter should experience significant deceleration during their early stages (Warmuth *et al.*, 2001). However, the low EIT cadence (12 minutes versus 1-2 minutes of the  $H\alpha$  observations) did not allow to directly check that in full detail. Note here that the majority of the EUV waves associated with Moreton waves in Warmuth (2010) shows evidence of deceleration (this could of course only be determined for events with EUV fronts visible in more than two images). Similar behavior is seen in SXR observations of coronal waves, when available. In cases for which the early EUV wave deceleration could have missed probably due to low cadence, the extrapolated Moreton wave track roughly matches that of the EUV wave later on during several events. These results suggest a strong relationship between Moreton waves and EUV waves.

The ultra-high AIA cadence allows for much more detailed comparisons between Moreton and EUV waves by combining AIA and  $H\alpha$  or He I 10830 Å observations, which will supply more detailed kinematics of both phenomena.

---

The first example of such a comparison is reported in Asai *et al.* (2012) where cospatial H $\alpha$  and EUV fronts were detected.

Note that AIA observations in the flare channels (94 and 131) may also help tracing EUV waves into lower temperatures. These channels, apart from their main peaks at very high temperatures, they have secondary weaker peaks at transition region temperatures. Therefore, if and whenever there is a wave extension towards lower temperatures, this could be searched by adding together several 94 or 131 Å images to bring up the signal to noise ratio.

10. *Establish the properties of off-limb wave-related oscillations.* These oscillatory phenomena are an excellent 'smoking gun' for the action of EUV waves. We need to fully characterize and map their properties, like period, amplitude, damping time etc, like done for individual oscillation events (e.g., Aschwanden and Schrijver, 2011). Determining in particular the initial phase of these oscillations and whether different oscillating structures are sharing or not the same initial phase could help into discriminating between different possibilities for their EUV wave origin (see Figure 7). Such analysis will also allow to infer detailed coronal seismology information over the large areas over the Sun that EUV waves are propagating. Moreover we can assess their contribution to the decay and the energetics of EUV waves.

**Acknowledgements** We thank the referee for the very useful comments. S.P. acknowledges support from an FP7 Marie Curie Re-integration Grant (FP7-PEOPLE-2010-RG/268288). He also thanks the Scientific Organising Committee of the "Sun-360: Stereo-4/SDO-2/SOHO-25 Workshop" for an invitation to give a talk on EUV waves which is the base of the present review. A.V. is supported by NASA contract S-136361-Y to the Naval Research Laboratory.

## References

- Arregui, I., Ballester, J.L.: 2011, *Space Sci. Rev.* **158**, 169. doi:10.1007/s11214-010-9648-9.
- Asai, A., Hara, H., Watanabe, T., Imada, S., Sakao, T., Narukage, N., Culhane, J.L., Doschek, G.A.: 2008, *Astrophys. J.* **685**, 622. doi:10.1086/590419.
- Asai, A., Ishii, T.T., Isobe, H., Kitai, R., Ichimoto, K., UeNo, S., Nagata, S., Morita, S., Nishida, K., Shiota, D., Oi, A., Akioka, M., Shibata, K.: 2012, *Astrophys. J. Lett.* **745**, L18. doi:10.1088/2041-8205/745/2/L18.
- Aschwanden, M.J., Schrijver, C.J.: 2011, *Astrophys. J.* **736**, 102. doi:10.1088/0004-637X/736/2/102.
- Aschwanden, M.J., Nitta, N.V., Wuelser, J.-P., Lemen, J.R., Sandman, A., Vourlidas, A., Colaninno, R.C.: 2009, *Astrophys. J.* **706**, 376. doi:10.1088/0004-637X/706/1/376.
- Attrill, G.D.R.: 2010, *Astrophys. J.* **718**, 494. doi:10.1088/0004-637X/718/1/494.

- 
- Attrill, G.D.R., Harra, L.K., van Driel-Gesztelyi, L., Démoulin, P., Wülser, J.-P.: 2007a, *Astronomische Nachrichten* **328**, 760. doi:10.1002/asna.200710794.
- Attrill, G.D.R., Harra, L.K., van Driel-Gesztelyi, L., Démoulin, P.: 2007b, *Astrophys. J. Lett.* **656**, L101. doi:10.1086/512854.
- Attrill, G.D.R., Engell, A.J., Wills-Davey, M.J., Grigis, P., Testa, P.: 2009, *Astrophys. J.* **704**, 1296. doi:10.1088/0004-637X/704/2/1296.
- Attrill, G.D.R., Harra, L.K., van Driel-Gesztelyi, L., Wills-Davey, M.J.: 2010, *Solar Phys.* **264**, 119. doi:10.1007/s11207-010-9558-8.
- Balasubramaniam, K.S., Cliver, E.W., Pevtsov, A., Temmer, M., Henry, T.W., Hudson, H.S., Imada, S., Ling, A.G., Moore, R.L., Muhr, N., Neidig, D.F., Petrie, G.J.D., Veronig, A.M., Vršnak, B., White, S.M.: 2010, *Astrophys. J.* **723**, 587. doi:10.1088/0004-637X/723/1/587.
- Ballai, I., Erdélyi, R., Pintér, B.: 2005, *Astrophys. J. Lett.* **633**, L145. doi:10.1086/498447.
- Berghmans, D., Hochedez, J.F., Defise, J.M., Lecat, J.H., Nicula, B., Slemzin, V., Lawrence, G., Katsyiannis, A.C., van der Linden, R., Zhukov, A., Clette, F., Rochus, P., Mazy, E., Thibert, T., Nicolosi, P., Pelizzo, M.-G., Schühle, U.: 2006, *Advances in Space Research* **38**, 1807. doi:10.1016/j.asr.2005.03.070.
- Biesecker, D.A., Myers, D.C., Thompson, B.J., Hammer, D.M., Vourlidas, A.: 2002, *Astrophys. J.* **569**, 1009. doi:10.1086/339402.
- Chen, F., Ding, M.D., Chen, P.F.: 2010, *Astrophys. J.* **720**, 1254. doi:10.1088/0004-637X/720/2/1254.
- Chen, F., Ding, M.D., Chen, P.F., Harra, L.K.: 2011, *Astrophys. J.* **740**, 116. doi:10.1088/0004-637X/740/2/116.
- Chen, P.F.: 2006, *Astrophys. J. Lett.* **641**, L153. doi:10.1086/503868.
- Chen, P.F., Wu, Y.: 2011, *Astrophys. J. Lett.* **732**, L20+. doi:10.1088/2041-8205/732/2/L20.
- Chen, P.F., Fang, C., Shibata, K.: 2005, *Astrophys. J.* **622**, 1202. doi:10.1086/428084.
- Chen, P.F., Wu, S.T., Shibata, K., Fang, C.: 2002, *Astrophys. J. Lett.* **572**, L99. doi:10.1086/341486.
- Cheng, X., Zhang, J., Olmedo, O., Vourlidas, A., Ding, M.D., Liu, Y.: 2012, *Astrophys. J. Lett.* **745**, L5. doi:10.1088/2041-8205/745/1/L5.
- Cohen, O., Attrill, G.D.R., Manchester, W.B. IV, Wills-Davey, M.J.: 2009, *Astrophys. J.* **705**, 587. doi:10.1088/0004-637X/705/1/587.

- 
- Culhane, J.L., Harra, L.K., James, A.M., Al-Janabi, K., Bradley, L.J., Chaudry, R.A., Rees, K., Tandy, J.A., Thomas, P., Whillock, M.C.R., Winter, B., Doschek, G.A., Korendyke, C.M., Brown, C.M., Myers, S., Mariska, J., Seely, J., Lang, J., Kent, B.J., Shaughnessy, B.M., Young, P.R., Simnett, G.M., Castelli, C.M., Mahmoud, S., Mapson-Menard, H., Probyn, B.J., Thomas, R.J., Davila, J., Dere, K., Windt, D., Shea, J., Hagood, R., Moye, R., Hara, H., Watanabe, T., Matsuzaki, K., Kosugi, T., Hansteen, V., Wikstol, Ø.: 2007, *Solar Phys.* **243**, 19. doi:10.1007/s01007-007-0293-1.
- Dai, Y., Auchère, F., Vial, J.-C., Tang, Y.H., Zong, W.G.: 2010, *Astrophys. J.* **708**, 913. doi:10.1088/0004-637X/708/2/913.
- Delaboudinière, J.-P., Artzner, G.E., Brunaud, J., Gabriel, A.H., Hochedez, J.F., Millier, F., Song, X.Y., Au, B., Dere, K.P., Howard, R.A., Kreplin, R., Michels, D.J., Moses, J.D., Defise, J.M., Jamar, C., Rochus, P., Chauvineau, J.P., Marioge, J.P., Catura, R.C., Lemen, J.R., Shing, L., Stern, R.A., Gurman, J.B., Neupert, W.M., Maucherat, A., Clette, F., Cugnon, P., van Dessel, E.L.: 1995, *Solar Phys.* **162**, 291. doi:10.1007/BF00733432.
- Delannée, C.: 2000, *Astrophys. J.* **545**, 512. doi:10.1086/317777.
- Delannée, C., Aulanier, G.: 1999, *Solar Phys.* **190**, 107. doi:10.1023/A:1005249416605.
- Delannée, C., Török, T., Aulanier, G., Hochedez, J.-F.: 2008, *Solar Phys.* **247**, 123. doi:10.1007/s11207-007-9085-4.
- Dolla, L.R., Zhukov, A.N.: 2011, *Astrophys. J.* **730**, 113. doi:10.1088/0004-637X/730/2/113.
- Downs, C., Roussev, I.I., van der Holst, B., Lugaz, N., Sokolov, I.V., Gombosi, T.I.: 2011, *Astrophys. J.* **728**, 2. doi:10.1088/0004-637X/728/1/2.
- Foullon, C., Verwichte, E., Nakariakov, V.M., Nykyri, K., Farrugia, C.J.: 2011, *Astrophys. J. Lett.* **729**, L8. doi:10.1088/2041-8205/729/1/L8.
- Gallagher, P.T., Long, D.M.: 2011, *Space Sci. Rev.* **158**, 365. doi:10.1007/s11214-010-9710-7.
- Gary, D.E., Dulk, G.A., House, L., Illing, R., Sawyer, C., Wagner, W.J., McLean, D.J., Hildner, E.: 1984, *Astron. Astrophys.* **134**, 222.
- Gilbert, H.R., Daou, A.G., Young, D., Tripathi, D., Alexander, D.: 2008, *Astrophys. J.* **685**, 629. doi:10.1086/590545.
- Golub, L., Deluca, E., Austin, G., Bookbinder, J., Caldwell, D., Cheimets, P., Cirtain, J., Cosmo, M., Reid, P., Sette, A., Weber, M., Sakao, T., Kano, R., Shibasaki, K., Hara, H., Tsuneta, S., Kumagai, K., Tamura, T., Shimojo, M., McCracken, J., Carpenter, J., Haight, H., Siler, R., Wright, E., Tucker, J., Rutledge, H., Barbera, M., Peres, G., Varisco, S.: 2007, *Solar Phys.* **243**, 63. doi:10.1007/s11207-007-0182-1.

- 
- Gopalswamy, N., Yashiro, S., Temmer, M., Davila, J., Thompson, W.T., Jones, S., McAteer, R.T.J., Wuelser, J.-P., Freeland, S., Howard, R.A.: 2009, *Astrophys. J. Lett.* **691**, L123. doi:10.1088/0004-637X/691/2/L123.
- Gopalswamy, N., Nitta, N., Akiyama, S., Mäkelä, P., Yashiro, S.: 2012, *Astrophys. J.* **744**, 72. doi:10.1088/0004-637X/744/1/72.
- Gosling, J.T., Hildner, E., MacQueen, R.M., Munro, R.H., Poland, A.I., Ross, C.L.: 1974, *J. Geophys. Res.* **79**, 4581. doi:10.1029/JA079i031p04581.
- Grechnev, V.V., Afanasyev, A.N., Uralov, A.M., Chertok, I.M., Eselevich, M.V., Eselevich, V.G., Rudenko, G.V., Kubo, Y.: 2011, *Solar Phys.*, 286. doi:10.1007/s11207-011-9781-y.
- Handy, B.N., Acton, L.W., Kankelborg, C.C., Wolfson, C.J., Akin, D.J., Bruner, M.E., Carvalho, R., Catura, R.C., Chevalier, R., Duncan, D.W., Edwards, C.G., Feinstein, C.N., Freeland, S.L., Friedlaender, F.M., Hoffmann, C.H., Hurlburt, N.E., Jurcevich, B.K., Katz, N.L., Kelly, G.A., Lemen, J.R., Levay, M., Lindgren, R.W., Mathur, D.P., Meyer, S.B., Morrison, S.J., Morrison, M.D., Nightingale, R.W., Pope, T.P., Rehse, R.A., Schrijver, C.J., Shine, R.A., Shing, L., Strong, K.T., Tarbell, T.D., Title, A.M., Torgerson, D.D., Golub, L., Bookbinder, J.A., Caldwell, D., Cheimets, P.N., Davis, W.N., Deluca, E.E., McMullen, R.A., Warren, H.P., Amato, D., Fisher, R., Maldonado, H., Parkinson, C.: 1999, *Solar Phys.* **187**, 229. doi:10.1023/A:1005166902804.
- Harra, L.K., Sterling, A.C.: 2003, *Astrophys. J.* **587**, 429. doi:10.1086/368079.
- Harra, L.K., Hara, H., Imada, S., Young, P.R., Williams, D.R., Sterling, A.C., Korendyke, C., Attrill, G.D.R.: 2007, *Pub. Astron. Soc. Japan* **59**, 801.
- Harra, L.K., Sterling, A.C., Gömöry, P., Veronig, A.: 2011, *Astrophys. J. Lett.* **737**, L4. doi:10.1088/2041-8205/737/1/L4.
- Hershaw, J., Foullon, C., Nakariakov, V.M., Verwichte, E.: 2011, *Astron. Astrophys.* **531**, A53+. doi:10.1051/0004-6361/201116750.
- Howard, R.A., Moses, J.D., Vourlidas, A., Newmark, J.S., Socker, D.G., Plunkett, S.P., Korendyke, C.M., Cook, J.W., Hurley, A., Davila, J.M., Thompson, W.T., St Cyr, O.C., Mentzell, E., Mehalick, K., Lemen, J.R., Wuelser, J.P., Duncan, D.W., Tarbell, T.D., Wolfson, C.J., Moore, A., Harrison, R.A., Waltham, N.R., Lang, J., Davis, C.J., Eyles, C.J., Mapson-Menard, H., Simnett, G.M., Halain, J.P., Defise, J.M., Mazy, E., Rochus, P., Mercier, R., Ravet, M.F., Delmotte, F., Auchere, F., Delaboudiniere, J.P., Bothmer, V., Deutsch, W., Wang, D., Rich, N., Cooper, S., Stephens, V., Maahs, G., Baugh, R., McMullin, D., Carter, T.: 2008, *Space Sci. Rev.* **136**, 67. doi:10.1007/s11214-008-9341-4.
- Hudson, H.S., Khan, J.I., Lemen, J.R., Nitta, N.V., Uchida, Y.: 2003, *Solar Phys.* **212**, 121. doi:10.1023/A:1022904125479.



- 
- Imada, S., Hara, H., Watanabe, T., Kamio, S., Asai, A., Matsuzaki, K., Harra, L.K., Mariska, J.T.: 2007, *Pub. Astron. Soc. Japan* **59**, 793.
- Innes, D.E., Genetelli, A., Attie, R., Potts, H.E.: 2009, *Astron. Astrophys.* **495**, 319. doi:10.1051/0004-6361:200811011.
- Jin, M., Ding, M.D., Chen, P.F., Fang, C., Imada, S.: 2009, *Astrophys. J.* **702**, 27. doi:10.1088/0004-637X/702/1/27.
- Khan, J.I., Aurass, H.: 2002, *Astron. Astrophys.* **383**, 1018. doi:10.1051/0004-6361:20011707.
- Kienreich, I.W., Temmer, M., Veronig, A.M.: 2009, *Astrophys. J. Lett.* **703**, L118. doi:10.1088/0004-637X/703/2/L118.
- Kienreich, I.W., Veronig, A.M., Muhr, N., Temmer, M., Vršnak, B., Nitta, N.: 2011, *Astrophys. J. Lett.* **727**, L43+. doi:10.1088/2041-8205/727/2/L43.
- Klassen, A., Aurass, H., Mann, G., Thompson, B.J.: 2000, *Astron. Astrophys. Suppl.* **141**, 357. doi:10.1051/aas:2000125.
- Kozarev, K.A., Korreck, K.E., Lobzin, V.V., Weber, M.A., Schwadron, N.A.: 2011, *Astrophys. J. Lett.* **733**, L25+. doi:10.1088/2041-8205/733/2/L25.
- Lemen, J.R., Title, A.M., Akin, D.J., Boerner, P.F., Chou, C., Drake, J.F., Duncan, D.W., Edwards, C.G., Friedlaender, F.M., Heyman, G.F., Hurlburt, N.E., Katz, N.L., Kushner, G.D., Levay, M., Lindgren, R.W., Mathur, D.P., McFeaters, E.L., Mitchell, S., Rehse, R.A., Schrijver, C.J., Springer, L.A., Stern, R.A., Tarbell, T.D., Wuelser, J.-P., Wolfson, C.J., Yanari, C., Bookbinder, J.A., Cheimets, P.N., Caldwell, D., Deluca, E.E., Gates, R., Golub, L., Park, S., Podgorski, W.A., Bush, R.I., Scherrer, P.H., Gummin, M.A., Smith, P., Auken, G., Jerram, P., Pool, P., Souffi, R., Windt, D.L., Beardsley, S., Clapp, M., Lang, J., Waltham, N.: 2012, *Solar Phys.* **275**, 17. doi:10.1007/s11207-011-9776-8.
- Li, T., Zhang, J., Yang, S., Liu, W.: 2012, *Astrophys. J.* **746**, 13. doi:10.1088/0004-637X/746/1/13.
- Linker, J.A., Lionello, R., Mikic, Z., Titov, V., Riley, P.: 2008, *AGU Spring Meeting Abstracts*, D5.
- Lionello, R., Linker, J.A., Mikić, Z.: 2009, *Astrophys. J.* **690**, 902. doi:10.1088/0004-637X/690/1/902.
- Liu, W., Nitta, N.V., Schrijver, C.J., Title, A.M., Tarbell, T.D.: 2010, *Astrophys. J. Lett.* **723**, L53. doi:10.1088/2041-8205/723/1/L53.
- Liu, W., Title, A.M., Zhao, J., Ofman, L., Schrijver, C.J., Aschwanden, M.J., De Pontieu, B., Tarbell, T.D.: 2011, *Astrophys. J. Lett.* **736**, L13+. doi:10.1088/2041-8205/736/1/L13.

- 
- Long, D.M., DeLuca, E.E., Gallagher, P.T.: 2011, *Astrophys. J. Lett.* **741**, L21+. doi:10.1088/2041-8205/741/1/L21.
- Long, D.M., Gallagher, P.T., McAteer, R.T.J., Bloomfield, D.S.: 2008, *Astrophys. J. Lett.* **680**, L81. doi:10.1086/589742.
- Long, D.M., Gallagher, P.T., McAteer, R.T.J., Bloomfield, D.S.: 2011, *Astron. Astrophys.* **531**, A42+. doi:10.1051/0004-6361/201015879.
- Ma, S., Wills-Davey, M.J., Lin, J., Chen, P.F., Attrill, G.D.R., Chen, H., Zhao, S., Li, Q., Golub, L.: 2009, *Astrophys. J.* **707**, 503. doi:10.1088/0004-637X/707/1/503.
- Ma, S., Raymond, J.C., Golub, L., Lin, J., Chen, H., Grigis, P., Testa, P., Long, D.: 2011, *Astrophys. J.* **738**, 160. doi:10.1088/0004-637X/738/2/160.
- Mann, G.: 1995, *J. Plasma Phys.* **53**, 109. doi:10.1017/S0022377800018043.
- McIntosh, S.W.: 2009, *Astrophys. J.* **693**, 1306. doi:10.1088/0004-637X/693/2/1306.
- Moses, D., Clette, F., Delaboudinière, J.-P., Artzner, G.E., Bougnet, M., Brunaud, J., Carabetian, C., Gabriel, A.H., Hochedez, J.F., Millier, F., Song, X.Y., Au, B., Dere, K.P., Howard, R.A., Kreplin, R., Michels, D.J., Defise, J.M., Jamar, C., Rochus, P., Chauvineau, J.P., Marioge, J.P., Catura, R.C., Lemen, J.R., Shing, L., Stern, R.A., Gurman, J.B., Neupert, W.M., Newmark, J., Thompson, B., Maucherat, A., Portier-Fozzani, F., Berghmans, D., Cugnon, P., van Dessel, E.L., Gabryl, J.R.: 1997, *Solar Phys.* **175**, 571. doi:10.1023/A:1004902913117.
- Muhr, N., Vršnak, B., Temmer, M., Veronig, A.M., Magdalenić, J.: 2010, *Astrophys. J.* **708**, 1639. doi:10.1088/0004-637X/708/2/1639.
- Muhr, N., Veronig, A.M., Kienreich, I.W., Temmer, M., Vršnak, B.: 2011, *Astrophys. J.* **739**, 89. doi:10.1088/0004-637X/739/2/89.
- Ofman, L., Thompson, B.J.: 2002, *Astrophys. J.* **574**, 440. doi:10.1086/340924.
- Ofman, L., Thompson, B.J.: 2011, *Astrophys. J. Lett.* **734**, L11+. doi:10.1088/2041-8205/734/1/L11.
- Olmedo, O., Vourlidas, A., Zhang, J., Cheng, X.: 2012, *Astrophys. J.*, *submitted*.
- Patsourakos, S., Vourlidas, A.: 2009, *Astrophys. J. Lett.* **700**, L182. doi:10.1088/0004-637X/700/2/L182.
- Patsourakos, S., Vourlidas, A., Kliem, B.: 2010, *Astron. Astrophys.* **522**, A100+. doi:10.1051/0004-6361/200913599.
- Patsourakos, S., Vourlidas, A., Stenborg, G.: 2010, *Astrophys. J. Lett.* **724**, L188. doi:10.1088/2041-8205/724/2/L188.

- 
- Patsourakos, S., Vourlidas, A., Wang, Y.M., Stenborg, G., Thernisien, A.: 2009, *Solar Phys.* **259**, 49. doi:10.1007/s11207-009-9386-x.
- Podladchikova, O., Vourlidas, A., Van der Linden, R.A.M., Wülser, J.-P., Patsourakos, S.: 2010, *Astrophys. J.* **709**, 369. doi:10.1088/0004-637X/709/1/369.
- Pohjolainen, S., Maia, D., Pick, M., Vilmer, N., Khan, J.I., Otruba, W., Warmuth, A., Benz, A., Alissandrakis, C., Thompson, B.J.: 2001, *Astrophys. J.* **556**, 421. doi:10.1086/321577.
- Pomoell, J., Vainio, R., Kissmann, R.: 2008, *Solar Phys.* **253**, 249. doi:10.1007/s11207-008-9186-8.
- Robbrecht, E., Patsourakos, S., Vourlidas, A.: 2009, *Astrophys. J.* **701**, 283. doi:10.1088/0004-637X/701/1/283.
- Rouillard, A.P., Odstrčil, D., Sheeley, N.R., Tylka, A., Vourlidas, A., Mason, G., Wu, C.-C., Savani, N.P., Wood, B.E., Ng, C.K., Stenborg, G., Szabo, A., St. Cyr, O.C.: 2011, *Astrophys. J.* **735**, 7. doi:10.1088/0004-637X/735/1/7.
- Schmidt, J.M., Ofman, L.: 2010, *Astrophys. J.* **713**, 1008. doi:10.1088/0004-637X/713/2/1008.
- Schrijver, C.J., Aulanier, G., Title, A.M., Pariat, E., Delannée, C.: 2011, *Astrophys. J.* **738**, 167. doi:10.1088/0004-637X/738/2/167.
- Selwa, M., Poedts, S., DeVore, C.R.: 2012, *Astrophys. J. Lett.* **747**, L21. doi:10.1088/2041-8205/747/2/L21.
- Sheeley, N.R., Hakala, W.N., Wang, Y.-M.: 2000, *J. Geophys. Res.* **105**, 5081. doi:10.1029/1999JA000338.
- St. Cyr, O.C., Plunkett, S.P., Michels, D.J., Paswaters, S.E., Koomen, M.J., Simnett, G.M., Thompson, B.J., Gurman, J.B., Schwenn, R., Webb, D.F., Hildner, E., Lamy, P.L.: 2000, *J. Geophys. Res.* **105**, 18169. doi:10.1029/1999JA000381.
- Temmer, M., Vršnak, B., Žic, T., Veronig, A.M.: 2009, *Astrophys. J.* **702**, 1343. doi:10.1088/0004-637X/702/2/1343.
- Temmer, M., Veronig, A.M., Gopalswamy, N., Yashiro, S.: 2011, *Solar Phys.*, 158. doi:10.1007/s11207-011-9746-1.
- Thernisien, A., Vourlidas, A., Howard, R.A.: 2009, *Solar Phys.* **256**, 111. doi:10.1007/s11207-009-9346-5.
- Thompson, B.J., Myers, D.C.: 2009, *Astrophys. J. Suppl.* **183**, 225. doi:10.1088/0067-0049/183/2/225.

- 
- Thompson, B.J., Plunkett, S.P., Gurman, J.B., Newmark, J.S., St. Cyr, O.C., Michels, D.J.: 1998, *Geophys. Res. Lett.* **25**, 2465. doi:10.1029/98GL50429.
- Thompson, B.J., Gurman, J.B., Neupert, W.M., Newmark, J.S., Delaboudinière, J.-P., St. Cyr, O.C., Stezelberger, S., Dere, K.P., Howard, R.A., Michels, D.J.: 1999, *Astrophys. J. Lett.* **517**, L151. doi:10.1086/312030.
- Thompson, B.J., Reynolds, B., Aurass, H., Gopalswamy, N., Gurman, J.B., Hudson, H.S., Martin, S.F., St. Cyr, O.C.: 2000, *Solar Phys.* **193**, 161.
- Tripathi, D., Raouafi, N.-E.: 2007, *Astron. Astrophys.* **473**, 951. doi:10.1051/0004-6361:20077255.
- Tsinganos, K.C.: 1980, *Astrophys. J.* **239**, 746. doi:10.1086/158160.
- Uchida, Y.: 1968, *Solar Phys.* **4**, 30. doi:10.1007/BF00146996.
- Žic, T., Vršnak, B., Temmer, M., Jacobs, C.: 2008, *Solar Phys.* **253**, 237. doi:10.1007/s11207-008-9173-0.
- Veronig, A.M., Temmer, M., Vršnak, B.: 2008, *Astrophys. J. Lett.* **681**, L113. doi:10.1086/590493.
- Veronig, A.M., Temmer, M., Vršnak, B., Thalmann, J.K.: 2006, *Astrophys. J.* **647**, 1466. doi:10.1086/505456.
- Veronig, A.M., Muhr, N., Kienreich, I.W., Temmer, M., Vršnak, B.: 2010, *Astrophys. J. Lett.* **716**, L57. doi:10.1088/2041-8205/716/1/L57.
- Veronig, A.M., Gomory, P., Kienreich, I.W., Muhr, N., Vrsnak, B., Temmer, M., Warren, H.P.: 2011, *Astrophys. J. Lett.* **743**, L10.
- Vourlidas, A., Patsourakos, S., Kouloumvakos, T.: 2011, In: *AAS/Solar Physics Division Abstracts #42*, 907.
- Vourlidas, A., Wu, S.T., Wang, A.H., Subramanian, P., Howard, R.A.: 2003, *Astrophys. J.* **598**, 1392. doi:10.1086/379098.
- Vourlidas, A., Howard, R.A., Esfandiari, E., Patsourakos, S., Yashiro, S., Michalek, G.: 2010, *Astrophys. J.* **722**, 1522. doi:10.1088/0004-637X/722/2/1522.
- Vršnak, B., Cliver, E.W.: 2008, *Solar Phys.* **253**, 215. doi:10.1007/s11207-008-9241-5.
- Vršnak, B., Lulić, S.: 2000, *Solar Phys.* **196**, 181.
- Vršnak, B., Warmuth, A., Brajša, R., Hanslmeier, A.: 2002, *Astron. Astrophys.* **394**, 299. doi:10.1051/0004-6361:20021121.

- 
- Vršnak, B., Magdalenic, J., Temmer, M., Veronig, A., Warmuth, A., Mann, G., Aurass, H., Otruba, W.: 2005, *Astrophys. J. Lett.* **625**, L67. doi:10.1086/430763.
- Vršnak, B., Warmuth, A., Temmer, M., Veronig, A., Magdalenic, J., Hillaris, A., Karlický, M.: 2006, *Astron. Astrophys.* **448**, 739. doi:10.1051/0004-6361:20053740.
- Wang, Y.-M.: 2000, *Astrophys. J. Lett.* **543**, L89. doi:10.1086/318178.
- Warmuth, A.: 2007, In: K.-L. Klein & A. L. MacKinnon (ed.) *Lecture Notes in Physics, Berlin Springer Verlag, Lecture Notes in Physics, Berlin Springer Verlag* **725**, 107.
- Warmuth, A.: 2010, *Adv. Space. Res.* **45**, 527. doi:10.1016/j.asr.2009.08.022.
- Warmuth, A., Mann, G.: 2005, *Astron. Astrophys.* **435**, 1123. doi:10.1051/0004-6361:20042169.
- Warmuth, A., Mann, G.: 2011, *Astron. Astrophys.* **532**, A151+. doi:10.1051/0004-6361/201116685.
- Warmuth, A., Mann, G., Aurass, H.: 2005, *Astrophys. J. Lett.* **626**, L121. doi:10.1086/431756.
- Warmuth, A., Vršnak, B., Aurass, H., Hanslmeier, A.: 2001, *Astrophys. J. Lett.* **560**, L105. doi:10.1086/324055.
- Warmuth, A., Vršnak, B., Magdalenic, J., Hanslmeier, A., Otruba, W.: 2004, *Astron. Astrophys.* **418**, 1101. doi:10.1051/0004-6361:20034332.
- West, M.J., Zhukov, A.N., Dolla, L., Rodriguez, L.: 2011, *Astrophys. J.* **730**, 122. doi:10.1088/0004-637X/730/2/122.
- White, S.M., Thompson, B.J.: 2005, *Astrophys. J. Lett.* **620**, L63. doi:10.1086/428428.
- Wills-Davey, M.J., Attrill, G.D.R.: 2009, *Space Sci. Rev.* **149**, 325. doi:10.1007/s11214-009-9612-8.
- Wills-Davey, M.J., Thompson, B.J.: 1999, *Solar Phys.* **190**, 467. doi:10.1023/A:1005201500675.
- Wills-Davey, M.J., DeForest, C.E., Stenflo, J.O.: 2007, *Astrophys. J.* **664**, 556. doi:10.1086/519013.
- Withbroe, G.L., Noyes, R.W.: 1977, *Annu. Rev. Astron. Astrophys.* **15**, 363. doi:10.1146/annurev.aa.15.090177.002051.
- Wu, S.T., Zheng, H., Wang, S., Thompson, B.J., Plunkett, S.P., Zhao, X.P., Dryer, M.: 2001, *J. Geophys. Res.* **106**, 25089. doi:10.1029/2000JA000447.

- 
- Yashiro, S., Gopalswamy, N., Michalek, G., St. Cyr, O.C., Plunkett, S.P., Rich, N.B., Howard, R.A.: 2004, *Journal of Geophysical Research (Space Physics)* **109**, 7105. doi:10.1029/2003JA010282.
- Zhang, J., Liu, Y.: 2011, *Astrophys. J. Lett.* **741**, L7. doi:10.1088/2041-8205/741/1/L7.
- Zhao, X.H., Wu, S.T., Wang, A.H., Vourlidas, A., Feng, X.S., Jiang, C.W.: 2011, *Astrophys. J.* **742**, 131. doi:10.1088/0004-637X/742/2/131.
- Zheng, R., Jiang, Y., Hong, J., Yang, J., Bi, Y., Yang, L., Yang, D.: 2011, *Astrophys. J. Lett.* **739**, L39+. doi:10.1088/2041-8205/739/2/L39.
- Zhukov, A.N.: 2011, *J. Atm. Solar-Terr. Res.* **73**, 1096. doi:10.1016/j.jastp.2010.11.030.
- Zhukov, A.N., Auchère, F.: 2004, *Astron. Astrophys.* **427**, 705. doi:10.1051/0004-6361:20040351.
- Zhukov, A.N., Rodriguez, L., de Patoul, J.: 2009, *Solar Phys.* **259**, 73. doi:10.1007/s11207-009-9375-0.